



Citation: Clark GT, Yu Y, Urban CA, Fu G, Wang C, Zhang F, et al. (2022) Circadian control of heparan sulfate levels times phagocytosis of amyloid beta aggregates. PLoS Genet 18(2): e1009994. https://doi.org/10.1371/journal.pgen.1009994

Editor: J. Nicholas Cochran, HudsonAlpha Institute for Biotechnology, UNITED STATES

Received: June 22, 2021

Accepted: December 14, 2021

Published: February 10, 2022

Copyright: © 2022 Clark et al. This is an open access article distributed under the terms of the Creative Commons Attribution License, which permits unrestricted use, distribution, and reproduction in any medium, provided the original author and source are credited.

Data Availability Statement: All data related to this manuscript has been placed on Mendeley Data (doi: 10.17632/zrmgjyggmr.1) and GitHub (https://github.com/gclark304/fluorescent_image_analysis).

Funding: This work was supported by an NIH-National Institute of Biomedical Imaging and Bioengineering Grant U01EB022546 (to J.M.H) (https://www.nibib.nih.gov/), an NIH-National Institute of General Medical Sciences Grant R35GM128687 (to J.M.H.) (https://www.nigms.nih.gov/), an National Science Foundation CAREER

RESEARCH ARTICLE

Circadian control of heparan sulfate levels times phagocytosis of amyloid beta aggregates

Gretchen T. Clark 1, Yanlei Yu², Cooper A. Urban 1, Guo Fu^{1,3}, Chunyu Wang 1,2,4, Fuming Zhang 4,5, Robert J. Linhardt 1,2,4,5, Jennifer M. Hurley 1,4*

- 1 Rensselaer Polytechnic Institute, Biological Sciences, Troy, New York, United States of America,
 2 Rensselaer Polytechnic Institute, Chemistry and Chemical Biology, Troy, New York, United States of America,
 3 Now at the Innovation and Integration Center of New Laser Technology, Chinese Academy of Sciences, Shanghai, China,
 4 Center for Biotechnology and Interdisciplinary Studies, Rensselaer Polytechnic Institute, Troy, New York, United States of America,
 5 Rensselaer Polytechnic Institute, Chemical and Biological Engineering, Troy, New York, United States of America
- * hurlej2@rpi.edu

Abstract

Alzheimer's Disease (AD) is a neuroinflammatory disease characterized partly by the inability to clear, and subsequent build-up, of amyloid-beta (A β). AD has a bi-directional relationship with circadian disruption (CD) with sleep disturbances starting years before disease onset. However, the molecular mechanism underlying the relationship of CD and AD has not been elucidated. Myeloid-based phagocytosis, a key component in the metabolism of A β , is circadianly-regulated, presenting a potential link between CD and AD. In this work, we revealed that the phagocytosis of A β 42 undergoes a daily circadian oscillation. We found the circadian timing of global heparan sulfate proteoglycan (HSPG) biosynthesis was the molecular timer for the clock-controlled phagocytosis of A β and that both HSPG binding and aggregation may play a role in this oscillation. These data highlight that circadian regulation in immune cells may play a role in the intricate relationship between the circadian clock and AD.

Author summary

Disruption of the 24-hour endogenous cycle that controls human behavior and cellular physiology, our circadian rhythms, has been correlated with an increase in both the rate and severity of Alzheimer's disease (AD), the currently incurable, costly, and steadily growing neurodegenerative disorder that affects millions of elderly patients. AD is a neurodegenerative, neuroinflammatory disease that is caused, in part, by the buildup of Amyloid-beta 42 (A β 42) plaques in the brain. To understand the mechanistic link between circadian disruption and AD, we studied the immune cells responsible for the clearance of A β 42 over circadian time. We found there was a daily oscillation in A β 42 clearance and that this oscillation was lost in cells without a circadian rhythm. We established the underlying cause of this oscillation was the circadian control of cell surface

Award 2045674 (to J.M.H.) (https://www.nsf.gov/), National Institutes of Health grants 1RF1AG069039 (to C.W.), DK111958 and CA231074 (to R.J.L.) (https://www.nih.gov/), Rensselaer Polytechnic Startup funds (to J.M.H.) (https://www.rpi.edu/), a gift from the Warren Alpert Foundation (to J.M.H.) (https://warrenalpert.org/), and a NIH-National Institute of Aging T32 Fellowship AG057464 (to G. T.C.) (https://www.nia.nih.gov/). The funders had no role in study design, data collection and analysis, decision to publish, or preparation of the manuscript.

Competing interests: The authors have declared that no competing interests exist.

molecules, heparan sulfate proteoglycans, which have previously been shown to play a role in the regulation of A β 42 clearance. We further showed that this regulation was specific to A β 42, demonstrating a mechanistic link underlying the connection between the disruption of circadian rhythms and AD.

Introduction

Alzheimer's Disease (AD) and Alzheimer's related dementias affect millions of people every year, are a leading cause of death in the U.S., and have associated care costs estimated at US \$818 billion globally [1,2]. AD is a neurodegenerative, neuroinflammatory disease that is characterized by extracellular β -amyloid (A β) plaques, intracellular hyperphosphorylated tau fibrils, and increased neuroinflammation [3]. Though targeting A β as a therapeutic strategy has met limited success, A β accumulation is still regarded as a crucial step in AD pathogenesis due to strong evidence from human genetics of familial AD and Down syndrome [4,5]. Thus, understanding the metabolism of A β is essential to understand AD mechanisms and develop AD therapies.

A physiological consequence (and perhaps causative factor) of AD is the disruption of the circadian clock, the 24-hour endogenous rhythm that tunes physiology to the day/night cycle [6-10] (S1 Fig). Correlated with this, there is a daily oscillation in the abundance of A β 42 in cerebrospinal fluid in healthy adults and this oscillation is ablated in patients with AD [6]. A key factor in the clearance of Aβ are the resident microglia and, in the later stages of AD, peripheral macrophages [7,11–13]. Increasing neuroinflammation due to the accumulation of Aβ42 plaques leads to elevated levels of macrophage markers, activating microglia and increasing peripheral macrophage migration across the blood brain barrier (BBB), where peripheral macrophages more efficiently clear Aβ42 [7,11–17]. A double-edged sword, increased microglial activation and peripheral macrophage migration enhances the already high levels of neuroinflammation, leading to heightened cell death and exacerbating disease phenotypes [18-25]. The circadian clock also exerts extensive influence over macrophage/microglial behavior and disruption of circadian regulation affects the ability of macrophages to phagocytize target particles [26–28] (S1 Fig). In total, the concordance of these factors points to a relationship between the circadian regulation of the immune system and AD through the metabolism of Aβ42. Despite the correlation between circadian Aβ42 abundance and circadian control of macrophage/microglial phagocytosis, the link between AD and the clock via the circadian timing of Aβ42 phagocytosis has not been examined.

In this report, we utilized bone-marrow derived macrophages (BMDM's) as a proxy for cells from the monocyte lineage to demonstrate that A β 42 phagocytosis is under circadian control. Transcriptomic and proteomic data from macrophages identified few components that are circadianly regulated in the classical phagocytosis pathways but highlighted oscillations in the enzymes of the biosynthesis pathways of cell surface proteoglycans (PGs), which are known to negatively regulate A β 42 clearance [28–30]. We validated that PG levels oscillated over circadian time in macrophages *in vitro*, with PG levels reaching their zenith antiphase to the zenith of A β 42 phagocytosis [29–35]. Chemically reducing PG levels ablated the circadian oscillation of A β 42 phagocytosis by enhancing A β 42 phagocytosis at its nadir. These data suggested that the presence of PGs suppresses the phagocytosis of A β 42 and our investigation into the mechanism behind this suppression showed that aggregation and PG binding were essential to the circadian regulation of A β 42 phagocytosis. Overall, our data suggests a

role for myeloid cells in the circadian timing of the clearance of A β 42 and an avenue through which the disruption of circadian rhythms can lead to enhanced AD pathogenesis.

Results

Phagocytosis of Aβ42 by Bone marrow derived macrophages is timed by the circadian clock

Aβ42 abundance oscillates with a circadian period, microglia and macrophages have been shown to phagocytize Aβ42, and phagocytosis by macrophages is under circadian regulation, leading us to hypothesize that oscillations in the metabolism of Aβ42 may stem from the circadian regulation of phagocytosis in cells from myeloid lineages [12,14,28]. To validate this theory, we first needed to demonstrate oscillations in the phagocytosis of Aβ42. To do so, we modified a previously-employed BMDM phagocytosis assay (as BMDMs are both models for activated microglia and are known to migrate into the brain in late-stage AD), to use fluorescently labeled A\u03b342 to determine if the phagocytosis of A\u03b342 is controlled by the circadian clock [28,36–38]. In brief, BMDMs were derived from bone marrow progenitor cells extracted from Per2::Luc C57BL/6J mice and differentiated with recombinant Macrophage Colony Stimulating Factor (M-CSF), with flow cytometry confirming complete differentiation into naïve peripheral macrophages [39,40]. These BMDMs were then serum-shock synchronized and luminescence traces confirmed that our protocol resulted in reliable, \sim 24-h, PER2 oscillations [28]. 16 h after synchronization, confluent dishes of these BMDMs were treated HiLyte 488 labeled Aβ42 (Anaspec), in triplicate, every 4 h over a 24 h circadian period. BMDMs treated with labeled Aβ42 were harvested two hours after Aβ42 treatment and fixed with formalin. Total cellular fluorescence levels were analyzed with fluorescent confocal microscopy and quantified using a custom cell measurement MATLAB script (Fig 1A, S2 Fig, and S1 Table).

Total cellular fluorescence levels demonstrated that the amount of Aβ42 phagocytized by macrophages underwent a daily oscillation, with the nadir occurring between 16 and 20 h post serum shock (PS) (CT8 in relation to the zenith of PER2-LUC) and the zenith at PS32 (CT20) [41] (Fig 1B and 1C, S1 Fig). The extended harmonic circadian oscillator model (ECHO version 4.1) was used to analyze the average of the three replicates from each timepoint and predicted that Aβ42 total cellular florescence, and therefore the phagocytosis of Aβ42, oscillated with a circadian period (~26 h, ECHO p-value = 1.61 x 10^{-6}) [42]. Additionally, when compared with PER2 levels extrapolated based on the lumicycle data of the macrophages sampled, we saw that total cellular fluorescence was highest after the zenith of PER2 levels [40] (Fig 1B and 1C). The Aβ42 phagocytosis experiment was then repeated using PER1^{-/-}/PER2^{-/-} knockout (KO) mice to confirm the circadian influence of this relationship. BMDMs from the knockout mice were extracted, derived into naïve macrophages, and synchronized as described above. KO macrophages were treated with fluorescently labeled Aβ42 for 2 h, in triplicate, every 4 h for 24 h starting at PS16. Total cellular fluorescence was quantified and showed an ablation of the zenith of fluorescence at PS32 (CT20), confirming that the clock regulates Aβ42 phagocytosis (S3 Fig).

Proteoglycan levels in macrophages undergo daily oscillations

We next used the ECHO program to probe our previously published, highly sampled/replicated, murine macrophage dataset, which tracked the transcriptome and proteome of BMDMs over two circadian days, to determine mechanisms that underlie the oscillation of A β 42 phagocytosis [28,42]. Many known pathways essential for A β 42 phagocytosis oscillated with a

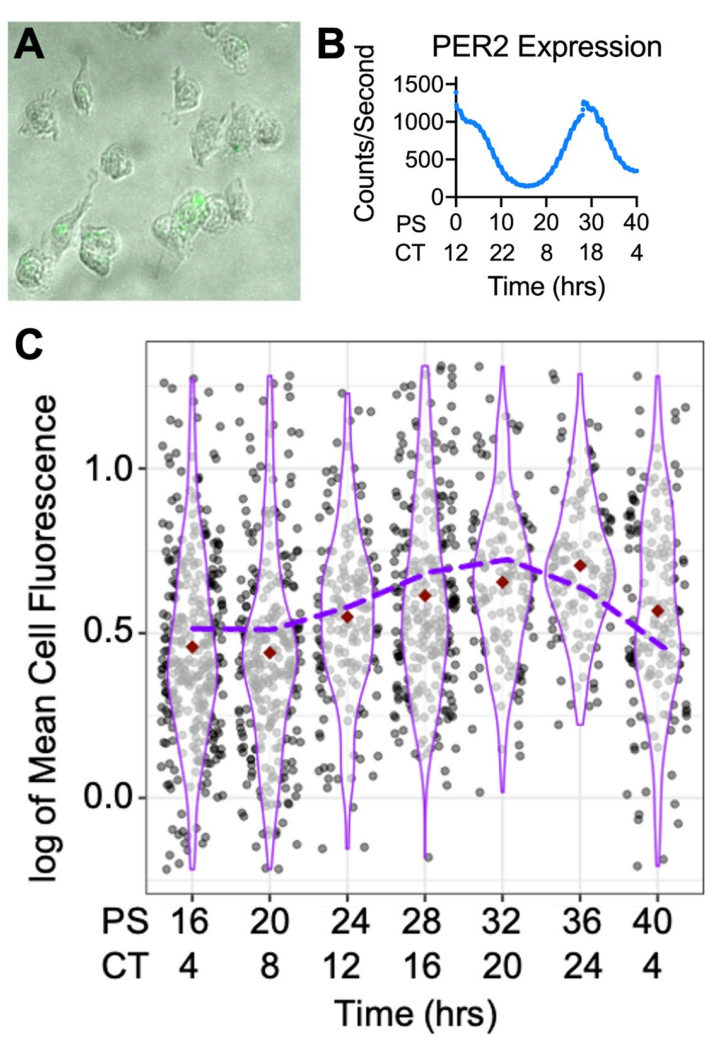


Fig 1. A β 42 phagocytosis oscillated with a circadian period. (A) Cropped composite image of fluorescent microscopy of the A β 42 treated macrophages. (B) PER2::LUC expression from untreated BMDMs, determined via bioluminescence using a lumicycle, reported in post shock (PS) and circadian time (CT). (C) Violin plot of A β 42 phagocytosis (n = 3) represented in logged mean cell fluorescence values plotted against post shock (PS) and circadian time (CT). Grey dots represent a single cell measurement, purple violin plot lines represent the range of the data, and red diamonds indicate the mean measurement of each time point. The purple dashed line depicts the ECHO fitted model of A β 42 phagocytosis. CT is in reference to the comparison of PER2 expression from Keller et al., 2009 [41] compared to PER2 expression from our cells. n = number of replicates.

circadian period at the transcript level, but we found no oscillation in the proteome associated with these pathways except for the low-density lipoprotein receptor (LDLR) (zenith at CT13) and the low-density lipoprotein receptor-related protein isoform 6 (LRP6) (zenith at CT1) [43,44] (S3 Table). However, neither of these proteins reached their zenith in-phase with the oscillation of A β 42 phagocytosis.

We then probed the two most enriched categories in the BMDM proteome according to Panther, binding and catalysis, and found several proteins related to proteoglycan (PG) synthesis and maintenance [45]. PGs are structurally diverse macromolecules that participate in a wide range of biological functions such as modulation of inflammation, extracellular matrix (ECM) assembly and remodeling, tissue repair, and ligand-receptor interactions [46,47]. PGs like heparan sulfate proteoglycans (HSPGs) and chondroitin sulfate proteoglycans (CSPGs)

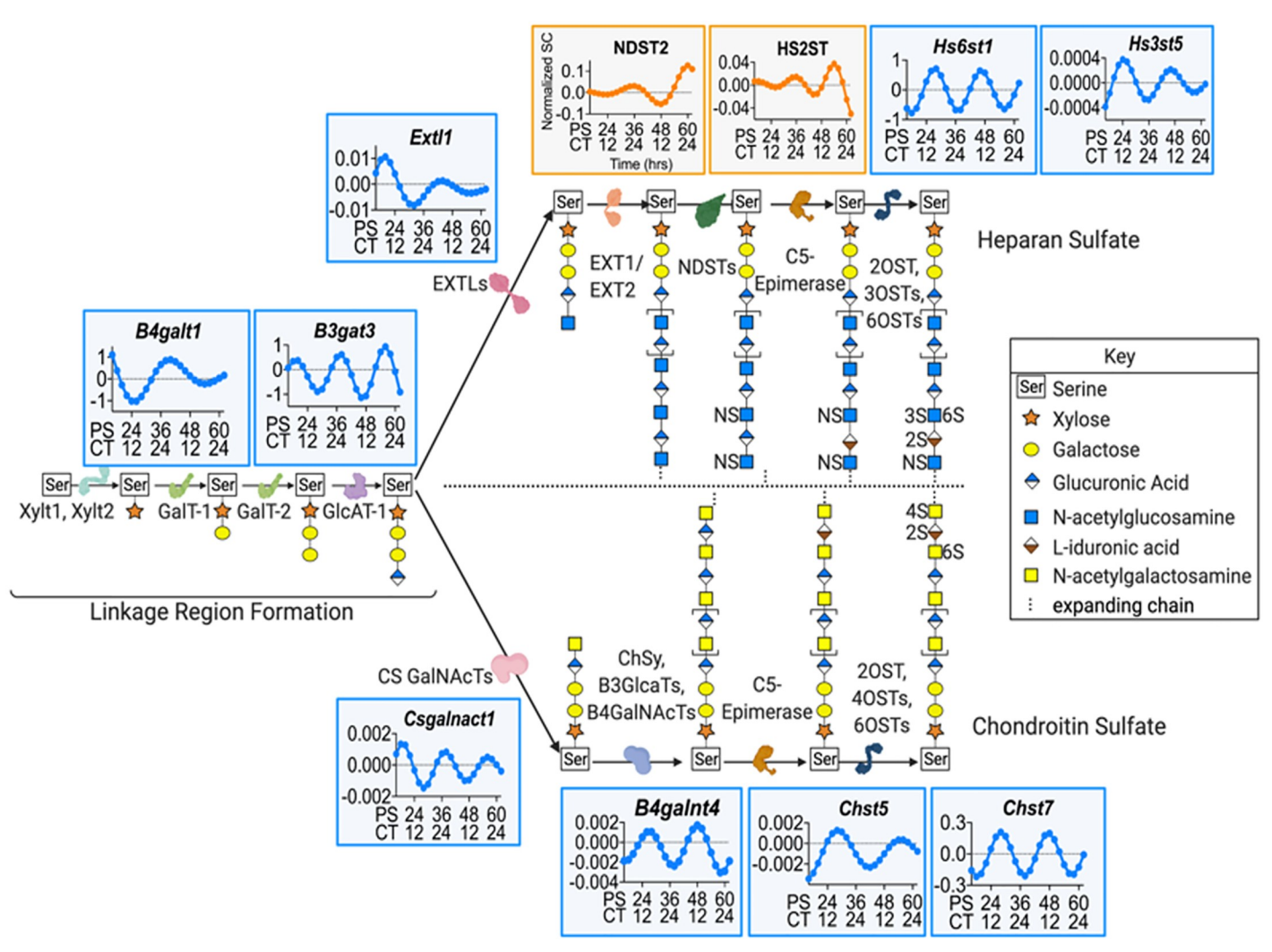


Fig 2. Enzyme levels in the HSPG and CSPG biosynthesis pathways varied over the circadian day. A diagrammatic representation of the pathways in HSPG and CSPG biosynthesis with the enzymes involved in each pathway that are under circadian regulation mapped to their location in the pathway. Pathways were adapted from Maeda, 2015 [54]; Kreuger and Kjellen, 2012 [55]; and Ly et al., 2011 [56]. The plotted expression graphs depict the ECHO fitted model of the gene expression for either RNA (blue) or protein (orange) over PS and CT. Representative HSPG and CSPG chains are shown.

are involved in the clearance of A β 42, associate with A β 42 to foster the formation of plaques, and reduce A β plaque load upon the knockout of a key enzyme in the HSPG biosynthesis pathway [29,30,31,33–35,48–51,52,53]. Using the published PG synthesis pathway from Maeda, 2015 [54], the HSPG synthesis pathway from Kreuger and Kjellen, 2012 [55], and the CSPG synthesis pathway from Ly et al., 2011 [56], we cross-referenced the PG synthesis pathway enzymes to the mouse genome using Mouse Genome Informatics (MGI) to establish the homologues for PG synthesis in mice [57]. Once potential PG biosynthesizing genes were identified, we mapped each protein (or transcript if the protein was not found in our dataset) in these pathways to the information from our circadian transcriptomic and proteomics data sets and found that some HSPG and CSPG biosynthesis enzymes undergo a daily oscillation at almost every step of PG biosynthesis in macrophages, from the formation of the linkage region to chain modification (Fig 2).

According to the current understanding of PG biosynthesis, creation of both HSPGs and CSPGs start with the formation of the linkage region by xylosyltransferases, XYLT1 and

XYLT2, which add a xylose to a serine. Following this, Galactosyltransferases, GALT-1 and GALT-2 (B4galt1 zenith at CT4.35), sequentially facilitate the addition of two galactose residues, followed by the glucuronosyltransferase, GLCAT-1 (Bgat3 zenith at CT7.1), catalyzed addition of glucuronic acid. The HSPG and CSPG biosynthesis pathways then diverge and both branch-point enzymes exostosin-like glycosyltransferase, EXTLs (Extl1 zenith at CT8.44), in the HSPG pathway and chondroitin sulfate N-acetylgalactosaminyltransferase, CS GALNACT (Csgalnact1 zenith at CT7.01), in the CSPG pathway are under the regulation of the circadian clock. HSPG chains undergo elongation through the alternating additions of glucuronic acid and N-acetylglucosamine by exostosin glycosyltransferases, EXT1 and EXT2, modification by N-sulfotransferases, NDSTs (NDST2 zenith at CT22.61), the conversion of D-glucuronic acid into L-iduronic acid by C5-epimerase, and the addition of sulfate groups by sulfotransferases (Hs6st1 zenith at CT15.53; Hs3st5 zenith at CT12.72; Hs2st zenith at CT4.37). In the CSPG pathway, CSPG elongation is catalyzed by chondroitin sulfate synthase, CHSY, along with glucuronosyl transferases, B3GLACTs, and N-acetyl galactosaminyl transferases, B4GALNACTs (B4Galnt4 zenith at CT14.87). The chain is then modified by C5-Epimerase, and various sulfotransferases (Chst5 zenith at CT16.71 and Chst7 zenith at CT16.11) add sulfate groups (Fig 2 and S2 Table). Clearly, many enzymes involved in the synthesis pathway for both HSPGs and CSPGs are tightly timed by the circadian clock and this could lead to an oscillation in HSPG and CSPG levels.

To confirm that the oscillations we noted in PG synthesizing enzymes lead to oscillations of PG levels in macrophages, we extracted bone marrow from Per2::Luc mice and differentiated the extracted monocytes into BMDMs. We then grew these BMDMs to confluency, synchronized using serum shock, and harvested the BMDMs in quadruplicate every 4 h for 24 h, beginning at 16 h PS. Additionally, spent media and extracellular matrix (ECM) scrapings were sampled at four timepoints over 24 h (S4A Fig). These samples were then analyzed using Liquid Chromatography Tandem Mass-Spectrometry (LC-MS/MS) for HSPG and CSPG disaccharides in various sulfation states (Fig 3). LC-MS/MS results were normalized by employing the CyQUANT cell proliferation assay at each time point to determine the total number of cells per pellet (S4B Fig).

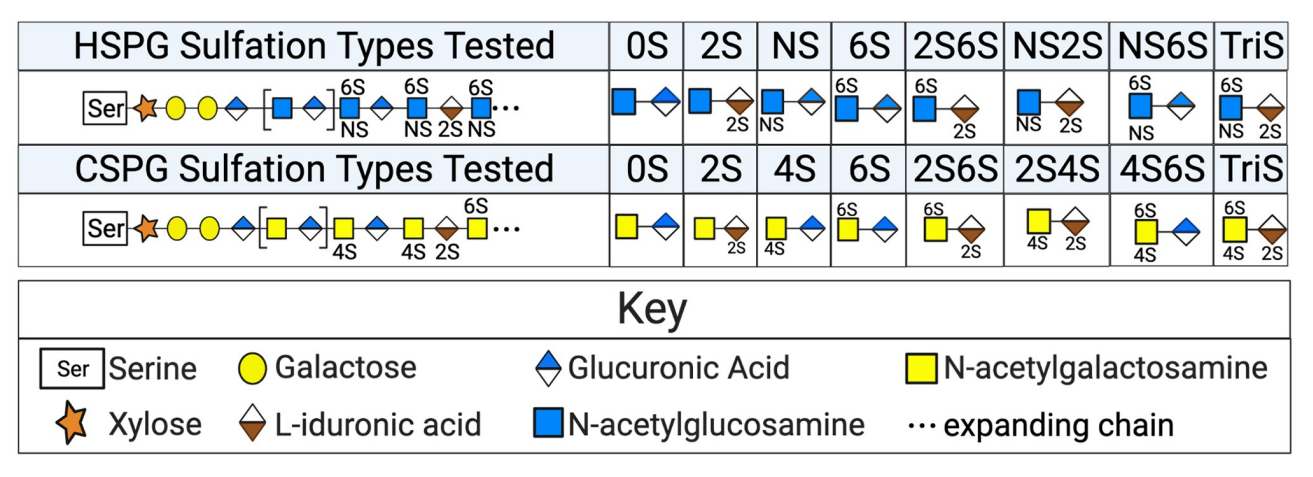


Fig 3. PG sulfation states quantified by LC-MS/MS. A schematic representation of the sulfation states tested in the cell samples, spent media, and ECM LC-MS/MS macrophage analysis. HSPGs investigated (top row) included 0S (no sulfation), 2S (sulfation on carbon 2), NS (sulfation on the amide), 6S (sulfation on carbon 6), 2S6S (sulfation on carbons 2 &6), NS2S (sulfation on the amide group and on carbon 2), NS6S (sulfation on the amide group and carbon 6), and TriS (sulfation on carbons 2 & 6 and on the amide group). CSPGs investigated (bottom row) include 0S (no sulfation), 2S (sulfation on carbon 2), 4S (sulfation on carbon 4), 6S (sulfation on carbon 6), 2S6S (sulfation on carbons 2 & 6), 2S4S (sulfation on carbon 2 & 4), 4S6S (sulfation on carbons 2, 4, and 6).

https://doi.org/10.1371/journal.pgen.1009994.g003

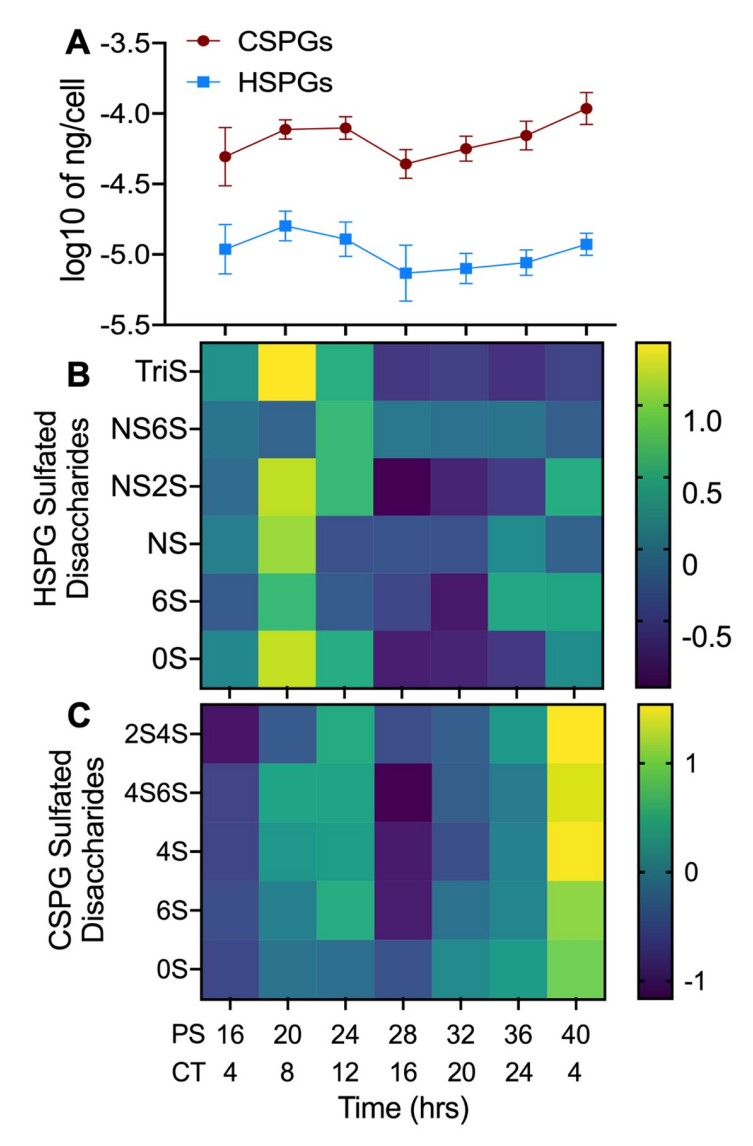


Fig 4. HSPG and CSPG levels in macrophages oscillated with a circadian period. (A) The sum of total cellular CSPG (n=4) and HSPG (n=4) levels (ng/cell) plotted against post shock (PS) and circadian time (CT). (B) Heat map of changes in cellular concentrations of specific HSPG sulfated disaccharides (n=4) shown in normalized Z-scores (relative levels) over PS and CT time. (C) Heat map of changes in the concentrations of specific CSPG sulfated disaccharides (n=4) shown in Z-scores over PS and CT. n=1 number of replicates, error bars represent the standard deviation of the replicates.

Our LC-MS/MS analysis of the macrophage cell pellet samples over circadian time demonstrated that, overall, the levels of both HSPGs and CSPGs oscillated with a circadian period (ECHO p-values = 1.30×10^{-7} and 1.62×10^{-7} for HSPGs and CSPGs, respectively) (Fig 4A). Overall, circadian oscillations in the levels of PGs synthesis and expression reached their zenith at or near PS20/CT8. Interestingly, the oscillation of Aβ42 phagocytosis occurred antiphase to HSPG and CSPG levels, suggesting the presence of PGs inhibited Aβ42 phagocytosis (compare Figs 1 to 4). As the phase of the transcripts and proteins that regulate the creation of HSPGs and CSPGs are discordant, it is clear the circadian timing of this process is highly complex and post-transcriptionally regulated (compare Figs 2 to 4).

When all detected species of HSPGs identified in the cell pellet (0S, 6S, NS, NS2S, TriS, and NS6S) were analyzed individually, they were all found by ECHO to oscillate with a circadian period (Fig 4B and S5A Fig, and S4 Table). Similarly, when the detected species of CSPGs identified in the cell pellet (2S4S, 4S6S, 4S, 6S, and 0S) were analyzed individually by ECHO (Fig 4C and S5D Fig, and S4 Table), they were all classified as oscillating with a circadian period. In the spent media samples, all detected HSPG and CSPG types (NS6S, NS2S, NS, and 0S for HSPGs and 0S, 4S, and 6S for CSPGs) were not found to be oscillating with a circadian period by ECHO (S5C and S5F Fig).

Finally, fewer HSPG and CSPG species were detected in the ECM scrapings (TriS, NS6S, NS2S, and 0S for HSPGs and 4S for CSPGs) and these species also appeared to have a daily oscillation (S5B and S5E Fig). We noted that in ECM samples the zenith in both HSPG and CSPG levels is at PS28 (S5B and S5E Fig). We also found in our proteomic data that proteins related to cell division such as cyclin dependent kinases, CDK1 and CDK2, CHK2 (a key regulator of cell cycle progress into mitosis), RAD21 (a cohesion complex component), and CDCA5 (Sororin, a chromatin-associated cohesion complex stabilizer), reached their zenith at PS28 [28,58–60] (S3 Table). As HSPGs and CSPGs are known to be involved in ECM remodeling, an essential step in mitosis, this implies that the timing of the zenith of ECM PGs may represent an additional link between cell division and the circadian clock [46,61,62].

Rhythmic phagocytosis of A β 42 is differentially regulated by high- and low-sulfated HSPGs

We hypothesized that the rhythmic oscillation of HSPGs may inhibit the phagocytosis of Aβ42 due to the antiphase relationship between Aβ42 phagocytosis and PG levels and the published repressive effect of HSPGs on Aβ42 phagocytosis [29,30] (Figs 1 and 4). To validate this hypothesis, we individually purified Heparinases I, II, and III, removed endotoxins, and confirmed Heparinase enzymatic activity (see Methods) [63-66] (S5 Table). Heparinase I cleaves between D-glucosamine and L-iduronic acid in highly sulfated regions, heparinase III cleaves between N-acetyl-D-glucosamine in low or unsulfated regions, and heparinase II cleaves in both positions [63]. We then extracted, derived, synchronized, and exposed BMDMs to fluorescently-labeled Aβ42 every 4 h over one circadian day. We next added a mixture of Heparinase I, II, and III to cleave all forms of HSPGs, with each biological replicate receiving a decreasing concentration of total heparinases (Replicate 1: 0.9577mg/ml of total heparinases, Replicate 2: 0.5071 mg/ml of total heparinases, Replicate 3: 0.2794 mg/ml of total heparinases) of the mixture of the three heparinases (see \$5 Table). Immediately following the addition of the heparinases, we added fluorescently labeled Aβ42 and sampled Aβ42 levels inside the cell 2 hours later. By using fluorescently labeled Aβ42, we controlled for endogenously generated Aβ, which can be affected by HSPG expression through its interaction with BACE1 processing of the amyloid precursor protein [67]. We found that regardless of Heparinase concentration, the addition of Heparinases I, II, and III ablated the oscillation in Aβ42 phagocytosis (average of all data points in Fig 4A, each treatment in S6C Fig). When comparing the relative levels of Aβ42 phagocytosis between the Heparinase treated and untreated macrophages, we found that Heparinase treatment increased phagocytosis when Aβ42 rhythmic phagocytosis reached its nadir (Heparinase Treatment PS20 vs A β 42 PS20 Welch's T-test p<2.2x10⁻¹⁶ and Hedges' g = 0.724791) but did not enhance overall levels of phagocytosis as compared to Aβ42-alone due to the low Hedges g value (Heparinase treatment PS32 vs A β 42 PS32 Welch's T-test p = 0.006426 and Hedges' g = 0.361095) (Fig 5). This data confirmed that circadianly-timed increases in the levels of HSPGs were rhythmically inhibiting the phagocytosis of Aβ42.

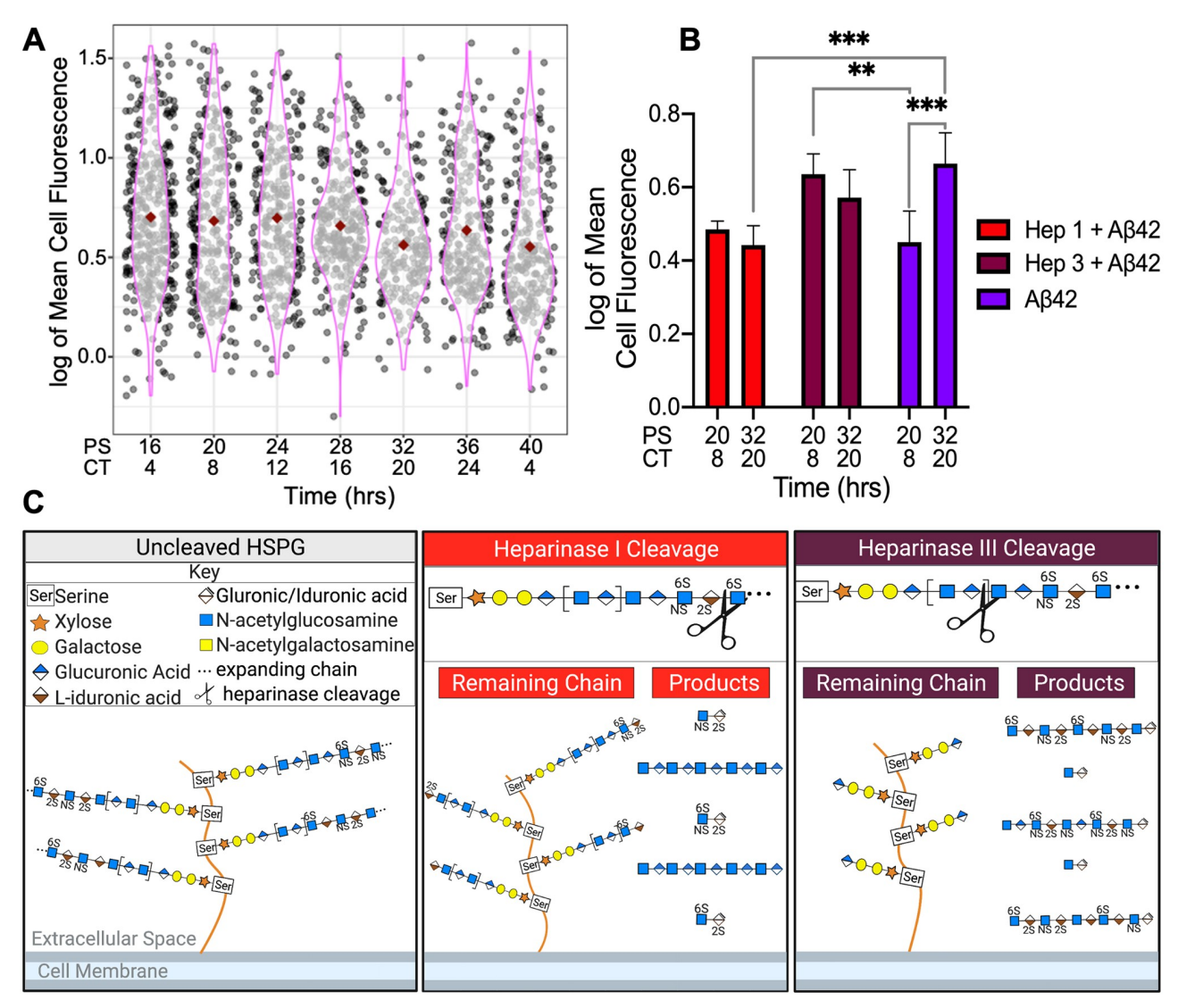


Fig 5. Heparinase treatment ablated daily oscillations in Aβ42 phagocytosis in macrophages. (A) A violin plot showing the phagocytosis of Aβ42 in the presence of a mixture of heparinases I, II, and III in logged mean fluorescence values plotted against PS and CT. Each cell sampled per time point is represented by a black or gray dot with the mean shown as a red diamond. The pink outline represents the range of values per timepoint. Note that data points from all the decreasing heparinase treatments were averaged to prepare this violin plot. (B) A bar graph comparing Aβ42 phagocytosis when heparinases I or III were added at PS20 (CT8) and PS32 (CT20). Red bars denote Heparinase 1 + Aβ42, maroon bars denote Heparinases 3 + Aβ42, purple bars denote Aβ42 without heparinases. All data shown was performed in triplicate (n>100 cells per replicate) and the error bars represent the standard deviation of the averaged replicates. *** = p < 2.2 x 10^{-16} and Hedge's G > 0.5 (C) Images depicting where individual heparinase cleave representative HSPG chains.

Notably, our data demonstrated that 0S HSPG was the predominant HSPG disaccharide in macrophages, indicating that macrophage HSPGs may have large unsulfated regions, which could be a factor in the circadian inhibition of A β 42 phagocytosis. To determine if our theory was correct, we next analyzed the phagocytosis of A β 42 at the zenith and nadir of A β 42 phagocytosis (PS20 and PS32) in the presence of either Heparinase III or Heparinase I only (based on Fig 4 and S4 Table). Isolated BMDMs, at PS20 and PS32 were treated in triplicate with HiLyte-488 labeled A β 42 and actively-equal amounts of either Heparinase I or Heparinase III and analyzed as described above (S5 Table). Heparinase I specifically cleaves between L-iduronic acid and N-acetylglucosamine on highly sulfated chains in HSPGs, leaving lower sulfated

chains bound to the cell surface. Heparinase III specifically cleaves between glucuronic acid and N-acetylglucosamine on lower-sulfated chains in HSPGs, leaving fragments of highly-sulfated heparan sulfate chains in the solution (Fig 5C).

We found that in macrophages that had been treated with Heparinase I, there was a loss of daily oscillation compared to untreated (Aβ42-Hep 1 PS20 vs PS32 Welch's T-test p = 0.08295 and Hedges' g = 0.101721; A β 42-alone PS20 vs PS32 Welch's T-test p = 8.979 x 10^{-15} and Hedges' g = 0.764648) and overall levels of phagocytosis significantly decreased at the circadian zenith, but not the nadir, as compared to Aβ42 phagocytosis in untreated macrophages (zenith: A β 42-Hep 1 PS32 vs A β 42-alone PS32 Welch's T-test p = 2.2 x 10⁻¹⁶ and Hedges' g = 0.635008; nadir: A β 42-Hep 1 PS20 vs A β 42-alone PS20 Welch's T-test p = 0.06002 and Hedges' g = 0.132791) (Fig 5 and S6A Fig). When macrophages were treated with Heparinase III, oscillations in Aβ42 phagocytosis were also ablated as compared to untreated (Aβ42-Hep 3 PS20 vs PS32 Welch's T-test p = 0.001997 and Hedges' g = 0.1663366). Conversely, phagocytosis increased at the nadir but not the zenith, as compared to Aβ42 phagocytosis in untreated macrophages (nadir: Aβ42-Hep 3 PS20 vs Aβ42-alone PS20 Welch's T-test p<2.2 x 10⁻¹⁶ and Hedges g = 0.5408882; zenith: A β 42-Hep 3 PS32 vs A β 42-alone PS32 Welch's T-test p =0.0007397 and Hedges' g = 0.21997) (Fig 5 and S6B Fig). Based on the previous study of the resultant cleavage products of Heparinase I and Heparinase III treatment of HSPGs, the differentially ablated circadian oscillations of Aβ42 phagocytosis upon heparinase I and heparinase III treatment suggests that the proper ratio of cell-surface sulfation states of HSPGs regulated the circadian timing of Aβ42 phagocytosis [63,68–70]. However, additional experiments to determine the degradation products afforded upon treatment with heparinase I and heparinase III would be required to confirm this supposition.

Binding of HSPGs to $A\beta$ peptides is a repressive factor in the circadian phagocytosis of $A\beta42$

Highly sulfated HSPGs, like perlecan, and CSPGs and dermatan sulfate PGs, having chondroitin-4S and dermatan sulfate GAG chains, have been shown to directly interact with AB [48,50,71]. PGs electrostatically bind a wide range of ligands and prefer basic amino acid residues with the highest preference for arginine, followed by lysine, and then to a much smaller extent, histidine. [72,73] The interaction between Aβ42 and heparan sulfate is known to occur through electrostatics from the dense negative charge of heparan sulfate and positively charged residues of Aβ42, particularly the HHQK cluster on Aβ42 (amino acids 13–16), which is included in the known heparin binding motif of Aβ XBBXBX where X is a hydropathic residue and B is a basic residue [73–79]. One important characteristic of Aβ42 binding to PGs is that upon binding, it changes its conformation and adopts a beta sheet structure, allowing it to rapidly aggregate [80–83]. Mouse A\(\beta\)2 (mA\(\beta\)42) is nearly identical to human A\(\beta\)42, with only three amino acid substitutions (R5G, Y10F, and H13R). However, these differences all reside within the known binding region to heparin, particularly the substitution of an arginine at the histidine residue, reside in or near the HHQK cluster and affects the interaction between HSPGs and mAβ42 as compared to human Aβ42 [73,77-79,84,85] (Fig 6C). This difference is important as while mice naturally produce mA\(\beta\)42, mA\(\beta\)42 plaques do not form and there is no natural occurrence of AD in mice, suggesting binding between HSPGs and Aβ42 may play a role in the development of AD disease phenotypes [86–88].

This led us to hypothesize that binding between HSPGs and Aβ42 at the cell surface may play a mechanistic role in the circadian phagocytosis of Aβ42. We therefore repeated our phagocytosis experiment using mouse HiLyte 488 labeled mAβ42 (Anaspec). Bone marrow derived from Per2::Luc mice was used to generate synchronized macrophages and, in

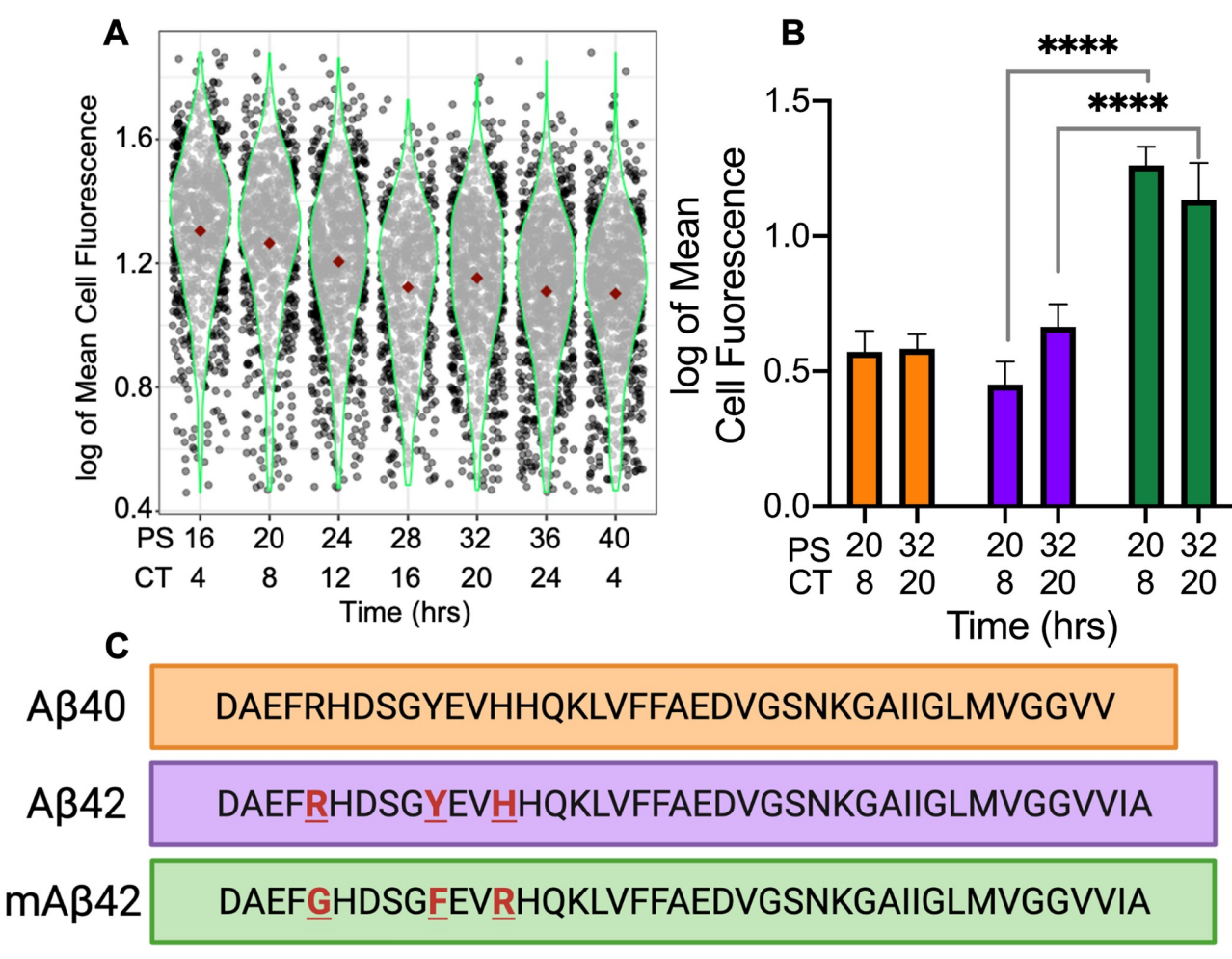


Fig 6. HSPG-regulated circadian macrophage phagocytosis was contingent upon HSPG-Aβ binding and aggregation. (A) Violin plot of mAβ42 phagocytosis represented in logged mean cell fluorescence values plotted against PS and CT. Grey dots represent a single cell measurement, green violin plot lines represent the range of the data, and red diamonds indicate the mean measurement of each time point. (B) A bar chart comparing Aβ40 phagocytosis (orange) to Aβ42 phagocytosis (purple) and mAβ42 phagocytosis (green) at PS20/CT8 and PS32/CT20. All data shown was performed in triplicate and the error bars represent the standard deviation of the replicates. **** = $p < 2.2 \times 10^{-16}$ and Hedge's g > 2.0 (C) An amino acid sequence comparison to show the differences between the Aβ42, Aβ40, and mAβ42 sequences.

triplicate, mA β 42 phagocytosis was assayed an analyzed as described above every 4 h for 24 h. mA β 42 phagocytosis did not have a circadian oscillation according to ECHO, suggesting that HSPG binding and subsequent conformational changes leading to rapid aggregation are essential for HSPG to impart circadian timing of A β 42 phagocytosis in macrophages [42,80–83] (Fig 6A). Aligned with our hypothesis, and with the data suggesting that HSPGs inhibit the phagocytosis of human but not mouse A β 42, the resulting data showed a significant increase in mA β 42 phagocytosis at the zenith and nadir of human A β 42 phagocytosis (mA β 42 PS20 vs A β 42 PS20 Welches T test p<2.2 x 10⁻¹⁶ and Hedges' g = 3.031588; mA β 42 PS32 vs A β 42 PS32 Welch's T test p<2.2 x 10⁻¹⁶ and Hedges g = 2.020813) as well as increased phagocytosis compared to human A β 42 phagocytosis at all sampled times [30] (Fig 6B). This data, correlated with the zenith in HSPG levels occurring at the nadir in A β 42 phagocytosis (Figs 1 and 4), suggested the circadian timing of increased cell-surface HSPG levels, and therefore interactions, negatively regulates the phagocytosis of A β 42.

Circadian phagocytosis of AB42 is correlated with AB42 plaque formation

In addition to binding A β 42, HSPGs regulate the formation of A β 42 plaques, with highly-sulfated HSPGs accumulating in the plaques [48,50,71,84,89]. A β peptides exist in two forms (A β 40 or A β 42) based on the cleavage of the amyloid precursor protein (APP) by β - and γ -secretase [90]. Previous studies show differential phagocytosis of A β 42 and A β 40, yet the key amino acids essential to binding are present in A β 40 (Fig 6C) (13–16, HHQK) [29,91]. However, the anionic bridge between lysine 28 and alanine 42, which is broken by HSPGs to allow the formation of A β 42 aggregates by rapidly changing its conformation from an alpha helix to a beta-sheet, does not occur immediately with A β 40, and thus HSPGs do not have an effect on A β 40 aggregation during short periods of interaction (< 1 day) [77,81,92]. Correlated with this, the A β 42 peptide shows higher aggregation kinetics and higher toxicity than A β 40 both as a free peptide and when bound to HSPGs [81,93].

Paired with our data showing an increase in phagocytosis when free highly-sulfated HSPG fragments are present (Fig 5), we hypothesized that if A β 42 aggregation was a key factor in HSPG timing of circadian phagocytosis, then there should be no oscillation in the phagocytosis of A β 40. We utilized our above-described phagocytosis assay to analyze the phagocytosis of A β 40 at the zenith and nadir times of A β 42 phagocytosis (PS20 and PS32) to determine if there was an oscillation in the phagocytosis of A β 40. We found no difference in A β 40 phagocytosis at PS20 and PS32 (A β 40 PS20 vs PS32 Welch's T-test p = 0.2362 and Hedges' g = 0.067337) confirming that there is no oscillation in A β 40 phagocytosis, and when we compared total phagocytosis of A β 40 at PS20 and PS32 to total phagocytosis of A β 42 at PS20 and PS32, we found no difference in overall phagocytosis due to the low Hedges' g value (A β 40 vs A β 42 Welch's T-test p = 1.278 x 10⁻⁰⁵ and Hedges' g = 0.275235). Overall, our results confirmed our hypothesis that the HSPG-regulated circadian-timing of A β 42 phagocytosis is also dependent upon A β 42 plaque formation (Fig 6B).

Discussion

The clearance of A β 42 is essential for a healthy neuronal microenvironment and accumulation of A β 42 is known to accelerate the development of the symptoms associated with AD [6,94]. The accumulation of A β 42 may in part be due to the impairment of the phagocytosis of A β 42 in Alzheimer's Disease model macrophages. As metabolism of A β 42 is controlled by the circadian clock *in vivo*, and aging and other cellular stresses are known to modulate the output of the circadian clock, it is logical to assume that disruption of oscillations in A β 42 metabolism due to AD-induced clock dysregulation could affect the accumulation of A β 42 [6,19,95,96]. This connection between the clock and A β 42 metabolism could provide a possible mechanism for the positive correlation between AD and circadian dysregulation [8,9,94]. To add to this connection, our results demonstrate circadian control of the phagocytosis of A β 42 in murine macrophages (Fig 1). As peripheral macrophages are models for microglia and also migrate to the brain in the later stages of AD, our findings suggest the disruption of the circadian timing of macrophage/microglia phagocytosis may be a vital component in A β 42 metabolism, highlighting a potential causative factor in the increase in accumulation of A β 42 in patients with clock/sleep disturbances [8,13,20,22,25,94,97].

Our analysis showed that a key factor in the circadian timing of A β 42 phagocytosis was the presence of cell-surface HSPGs (Fig 7). LC-MS/MS analysis of macrophages over circadian time showed a distinct rhythm in HSPG levels (Figs 2 and 4). The zenith and nadirs of the HSPG oscillation were antiphase to those of A β 42 phagocytosis, suggesting that HSPGs play an inhibitory role in the phagocytosis of A β 42 (Fig 7). The removal of all HSPG chains by treating synchronized macrophages with Heparinase I, II and III ablated the rhythm in the

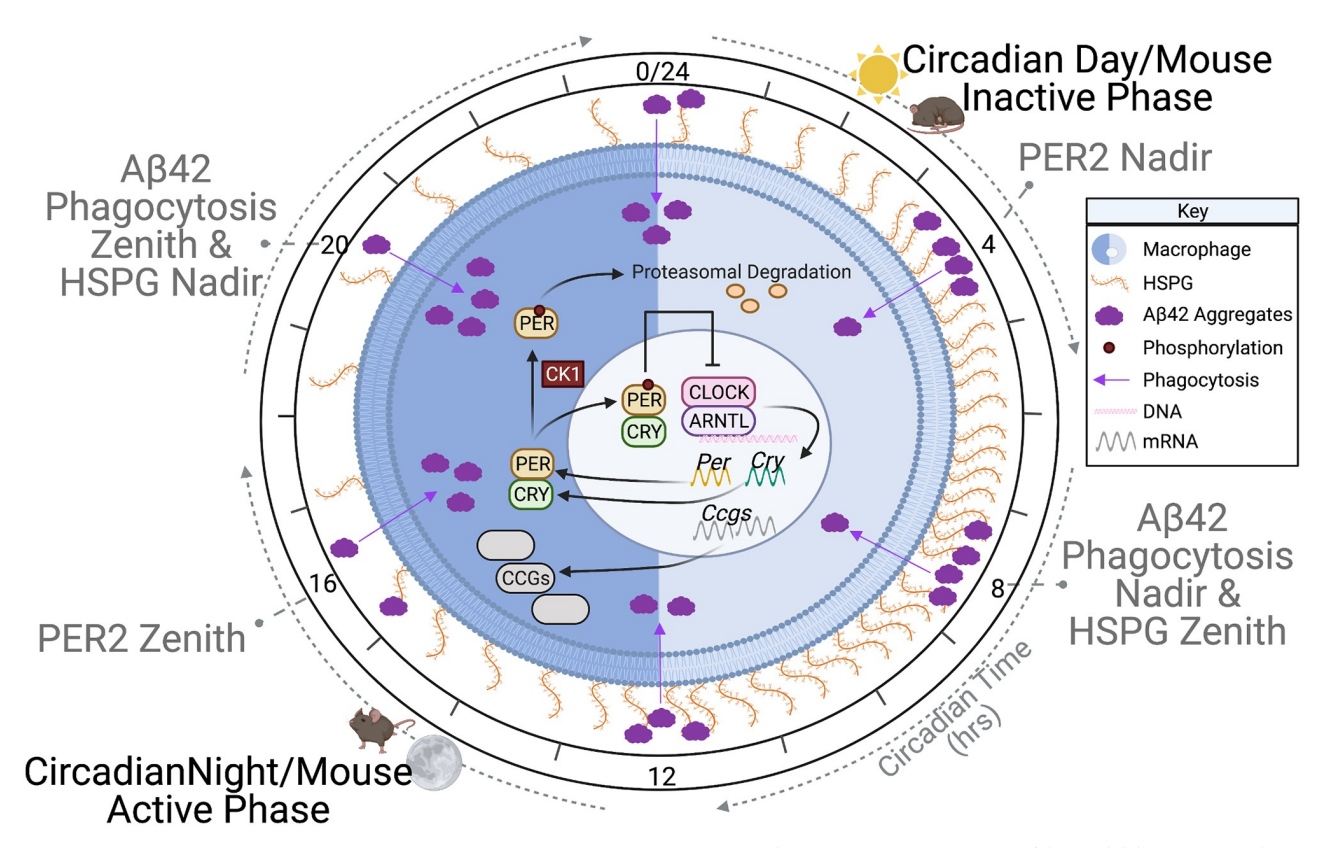


Fig 7. Circadian regulation of cell surface HSPGs time amyloid-beta phagocytosis. A diagrammatic representation of the model demonstrating how cell surface HSPGs regulate the phagocytosis of amyloid-beta. As time progresses from CT0, HSPGs (orange) increase on the cell surface of a macrophage (blue) and decrease the phagocytosis of amyloid-beta (purple), reaching a nadir in phagocytosis at CT8. Near CT12, HSPG levels decrease, and amyloid-beta phagocytosis rises, with the zenith in phagocytosis at CT20. Superimposed on the macrophage is a simplified version of the transcription/translation negative feedback loop that drives the oscillation of HSPG levels. The phases of mouse activity are shown in parallel with the HSPG levels.

oscillation of A β 42 phagocytosis by increasing phagocytosis at the nadir, cementing the importance of HSPGs in the circadian timing of A β 42 clearance (Fig 5). Previous studies have shown differential effects of HSPG species on A β 42, and our data paralleled this as we found that it is the presence of HSPGs or lack thereof is essential for the circadian timing of phagocytosis, though the complexity of the resultant HSPG fragments after individual Heparinase treatment made determining these roles difficult [50,52,53,98–100] (Fig 5). While HSPGs have previously been implicated in multiple pathways of A β clearance, cellular toxicity, and plaque generation, our work is the first to demonstrate a link between the circadian timing of HSPGs and A β 42 clearance [48,50,67,100–102].

The relationship between A β 42 clearance and HSPG binding has been shown, with HSPGs, perlecan, and syndecans binding A β 42, regulating A β 42 toxicity [49,84,102,103]. Highly sulfated HSPGs bind A β 42 both extracellularly or at the cell surface to affect phagocytosis [71,100,104]. Additionally, HSPGs play a role in other A β 42 clearance pathways, i.e., receptor mediated endocytosis, in neurons and glia cells [105,106]. We predict that the circadianly-timed increase in HSPGs on the cell surface could affect HSPG/A β 42 binding and this binding could be the mechanistic cause of the temporal inhibition in A β 42 phagocytosis. Our data showing that the overall phagocytosis of mA β 42, which contains mutations in the binding region specific to HSPGs, was higher and had no oscillation compared to human A β 42, supports this theory [77,84,85] (Fig 6). We theorize the HSPG-correlated inhibition of A β 42 phagocytosis is due to

HSPG-induced A β 42 aggregation on the cell surface, which can inhibit protease degradation of A β 42 and/or receptor mediated endocytosis of A β 42 [81,107]. Correlated with this, microglial phagocytosis and sequestration of A β in lysosomes has been shown to promote plaque formation [108] (Fig 1). Therefore, the suppression of phagocytosis at non-advantageous circadian times through the binding of A β 42 to cell surface HSPGs may be important to preventing intracellular plaque formation, which is known to lead to cellular toxicity [109].

Congruently, A β 42 plaque formation has been positively correlated to the presence of HSPGs [53,71,100]. Previous studies have shown that low-sulfated HSPGs did not enhance A β 42 plaque formation and lack of N-sulfated heparin reduced A β phagocytosis [50]. Our work correlated with this, as the phagocytosis of A β 40, which forms far fewer plaques than A β 42, has no circadian oscillation in phagocytosis, suggesting that plaque formation is also correlated with circadian phagocytosis of A β 42 [90] (Fig 6). A β 40 had similar levels of overall phagocytosis as compared to A β 42, though this is possibly due to solubility differences as microglia readily clear soluble A β , or due to energy independent endocytosis of A β 40, which has been demonstrated in neurons [110–113]. Moreover, when we released HSPGs from the cell surface using Heparinase III, making long sulfated HSPG chain fragments readily available for the formation of aggregates off of the cell surface, we saw an increase in phagocytosis at the nadir, supporting this hypothesis [89] (Fig 5). Furthermore, the source of HSPGs involved in plaque formation is hypothesized to be from microglia and macrophages, providing a further potential connection between AD, the circadian clock, and the immune system [114–116].

Beyond the discovery of the circadian timing of Aβ42 phagocytosis by HSPGs, there is a striking amount of circadian regulation devoted to timing oscillations in the levels of all PGs (Fig 4). We found that the circadian clock controlled many elements of the pathways that regulate the production of HSPGs and CSPGs, with 16.67% of identified proteins and 38.33% of identified RNAs in the pathway oscillating with a circadian rhythm (Fig 2). Much of this regulation was differential between the transcript and protein levels, in parallel with the findings from Collins et al 2021, suggesting that circadian post-transcriptional regulation is key to this process [28]. As PGs are key regulators for cell surface interactions in the inflammatory response, the circadian regulation of PGs in macrophages has strong implications for inflammation and immunity beyond its affect in AD [117]. Macrophage polarization, which is also controlled by the circadian clock, results in differently expressed HSPGs, with less 2S and 6S sulfation when pushed into the M1 or inflammatory state [114,118,119]. This implies that the circadian regulation of HSPG and CSPG expression could be critical to preventing a hyper inflamed state in inflammatory diseases such as AD. Moreover, as PGs play critical roles in development and cellular processes, it is likely that PGs fall under the regulation of the circadian clock in other tissue types, making it a promising target for future circadian studies [117,120,121].

Methods

Ethics statement

The experiments conducted with mice were done in accordance with the guidelines set by the National Institutes of Health Office of Intramural Research and were approved and supervised by the Rensselaer Polytechnic Institute Animal Care and Use Committee (protocol number HUR-001-18).

Animals

PER2::LUC C57BL/6J male mice 3–6 months of age bred from Jackson Labs stock strains (Accession # 006852) were used for all WT experiments and were euthanized using CO₂ gas

and cervical dislocation [40]. Per2::Luc C57BL/6J mice were kept on a strict lighting schedule of 12L:12D to maintain synchronized circadian rhythms and fed standard rodent chow *ad libitum*. PER1^{-/-}/PER2^{-/-} knockout male mice 3–6 months in age were used in all KO experiments and were euthanized using CO₂ gas and cervical dislocation [122]. PER1^{-/-}/PER2^{-/-} mice were kept on a strict 12L:12D lighting schedule and were fed antibiotic rodent chow *ad libitum* due to a *Helicobacter* infection in this mouse line.

Reagents

Amyloid-beta 42 labeled with HiLyte 488 (AS-60479-01), Amyloid-beta 40 labeled with HiLyte 488 (AS-60491-01), and custom Mouse amyloid-beta 42 labeled with HiLyte 488 (SQ-ANCPXXXX) were all purchased from Anaspec (Fremont, CA, USA). ACK lysing buffer (10-548E) was manufactured by Lonza.

Media

For macrophage differentiation media, DMEM media (Corning 10-013-CV) was used and supplemented with fetal bovine serum (FBS) (Gibco 10437028) at a 1:10 dilution, 100x Penstrep at a 1:100 dilution (Corning MT30002CI), 200mM L-glutamine at a 1:100 dilution (Corning 25-005-CI), Beta-mercaptoethanol (BME) at a 1:1000 dilution (Gibco 21985–023), and 50 mg/ml Gentamicin at a 1:1000 dilution (Gibco 15750–060).

For macrophage assay medium (after serum shock), Leibovitz media (Gibco 21083–027) was used and supplemented with fetal bovine serum (FBS) at a 1:10 dilution (Gibco 10437028), 100x Penstrep at a 1:100 dilution (Corning MT30002CI), 200mM L-glutamine at a 1:100 dilution (Corning 25-005-CI), Beta-mercaptoethanol (BME) at a 1:1000 dilution (Gibco 21985–023), 1 M HEPES at a 1:100 dilution (Gibco 15630–080), 50 mg/ml Gentamicin at a 1:1000 dilution (Gibco 15750–060), and Luciferin at a 1:100 ratio supplied by (Gold Biotechnology LUCK-1G) when appropriate.

For macrophage serum starvation assay media, Leibovitz media (Gibco 21083–027) was used and supplemented with 100x Penstrep at a 1:100 dilution (Corning MT30002CI), 200 mM L-glutamine at a 1:100 dilution (Corning 25-005-CI), Beta-mercaptoethanol (BME) at a 1:1000 dilution (Gibco 21985–023), 1 M HEPES at a 1:100 dilution (Gibco 15630–080), and 50 mg/ml Gentamicin at a 1:1000 dilution (Gibco 15750–060).

For macrophage serum shock media, Leibovitz media (Gibco 21083–027) was used and supplemented with FBS at a 50% dilution (Gibco 10437028), 100x Penstrep at a 1:100 dilution (Corning MT30002CI), 200 mM L-glutamine at a 1:100 dilution (Corning 25-005-CI), Beta-mercaptoethanol (BME) at a 1:1000 dilution (Gibco 21985–023), 1M HEPES at a 1:100 dilution (Gibco 15630–080), and 50mg/ml Gentamicin at a 1:1000 dilution (Gibco 15750–060).

All cell culture medias contained Macrophage Colony Stimulating Factor (M-CSF) at a 1:1000 dilution (Prospec cyt-439-c). Phosphate buffered saline (PBS) (Corning 21-040-CV) was used to wash the cells in between media changes. Cell Stripper (Corning 25-056-CI) was used to remove the adherent macrophages from cell culture dishes for harvesting. Buffered formalin phosphate (Fisher Chemical SFL004) was used for fixing harvested cells.

Mass spectrometry standards

Unsaturated disaccharide standards of CS ($0S_{CS-O}$: ΔUA -GalNAc; $4S_{CS-A}$: ΔUA -GalNAc4S; $6S_{CS-C}$: ΔUA -GalNAc6S; $2S_{CS}$: $\Delta UA2S$ -GalNAc; $2S4S_{CS-B}$: $\Delta UA2S$ -GalNAc4S; $2S6S_{CS-D}$: $\Delta UA2S$ -GalNAc6S; $4S6S_{CS-E}$: ΔUA -GalNAc4S6S; $4S6S_{CS-E}$: ΔUA -GalNAc4S6S; $4S6S_{CS-E}$: ΔUA -GalNAc4S6S, (Iduron, CD001, CD002, CD003, CD004, CD005, CD006, CD007 and CD008, respectively),

unsaturated disaccharide standards of HS ($0S_{HS}$: ΔUA -GlcNAc; NS_{HS}: ΔUA -GlcNS; 6S_{HS}: ΔUA -GlcNAc6S; 2S_{HS}: ΔUA 2S-GlcNAc; 2SNS_{HS}: ΔUA 2S-GlcNS; NS6S_{HS}: ΔUA 2S-GlcNS6S; 2S6S_{HS}: ΔUA 2S-GlcNAc6S; TriS_{HS}: ΔUA 2S-GlcNS6S), and unsaturated 1,3-linked disaccharide standard of HA ($0S_{HA}$: ΔUA -GlcNAc), (Iduron, HD006, HD005, HD008, HD007, HD002, HD004, HD003, HD001 and HA02, respectively) were purchased from Iduron, UK, where ΔUA is 4-deoxy- α -L-threo-hex-4-enopyranosyluronic acid.

Enzymes

Chondroitin lyase ABC from *Proteus vulgaris* was expressed in the Linhardt laboratory (see below). Recombinant *Flavobacterial* heparin lyases I, II, and III were expressed in the Linhardt laboratory using *Escherichia coli* strains provided by Jian Liu (College of Pharmacy, University of North Carolina).

Chemicals

2-Aminoacridone (AMAC) (Sigma-Aldrich 06627) and sodium cyanoborohydride (NaCNBH₃) (Sigma-Aldrich 156159) Calcium chloride (449709), DMSO (Sigma-Aldrich 94563), acetic acid (Sigma-Aldrich A6283), ammonium acetate (Sigma-Aldrich 73594) and methanol (Sigma-Aldrich 646377) were obtained from Sigma-Aldrich (St. Louis, MO, USA).

Bone marrow derived macrophage extraction and synchronization

Bone marrow was harvested from the femurs and tibias of one 3-6-month-old male mouse using a 26 g needle and syringe filled with DMEM supplemented media. ACK lysing buffer (Lonza 10-548E) was used to lyse red blood cells in order to prevent erythrocyte contamination. Filtered bone marrow cells were counted using a BioRad TC20 automated cell counter and plated on 35 mm cell culture plates at a density of 1 x 10⁶ in macrophage differentiation media. After three days of incubation at 37°C with 5% CO₂, fresh macrophage differentiation media was added. After another 3 days of incubation, the cells were washed with 2 ml warm PBS per plate, and replaced with macrophage assay media, and the cultures were incubated for 24 h. Macrophage cultures were then washed with 2 ml warm PBS, macrophage serum starvation media was added, and the plates were incubated in the starve media for 24 h. Next, macrophage serum starvation media was removed, and macrophage serum shock media was added, and cultures were incubated for 2 h [123]. Macrophage cultures were then washed with 2 ml warmed PBS each and macrophage media Luciferin was added. Cultures were sealed with grease and glass cover slips and placed in a LumiCycle 32 luminometer (Actimetrics) to confirm synchronization of circadian rhythmicity. Assays began 16 h post serum shock to allow the synchronized cells to return to homeostasis.

Amyloid-beta reconstitution

All amyloid-beta isoforms were reconstituted 24 h or less before experimentation in water and PBS (1:1) and were dissolved using sonication for approximately 30 min. The reconstituted A β was pooled from individual vials before aliquoting for each experimental replicate. The aliquots were then flash frozen and stored at -80°C until 20 min before use.

Phagocytosis assay

Using synchronized macrophages (as described above) starting at PS16 macrophages were treated every 4 h for 24 h, in triplicate, with 115 μ l (0.25 mg/ml) of fluorescently labeled amyloid-beta (PS16, PS20, PS24, PS28, PS32, PS36, and PS40) and heparinases at the reported

activity levels (S5 Table). The treated macrophages were then incubated at 37°C for 2 h. Following the two-hour incubation, the media was aspirated, and the macrophages were washed with 2ml of PBS three times before Cell Stripper (Corning 25-056-CI) was added to the cultures, which were then incubated at 37°C for 3 min. Detached macrophages were next centrifuged at 400 g for 5 min, the supernatant was aspirated, and the macrophage cell pellets were resuspended in formalin and incubated in the dark at room temperature for 30 min. Macrophages were then centrifuged for 5 min at 400 g, the supernatant was aspirated, and the macrophages were resuspended in 250 μ L of PBS and kept at 4°C. The fixed macrophages were imaged using fluorescent microscopy within a week of the experiment. All fluorescent images from the phagocytosis experiments are available on Mendeley Data (doi: 10.17632/zmgjyggmr.1).

Fluorescent image analysis

Macrophage cells containing fluorescent A β were imaged on a Zeiss LSM 510 Laser scanning confocal microscope using the 40x objective and an argon laser at 488nm excitation wavelength. Macrophages were viewed in two channels, the light channel and the fluorescent channel and microscope settings were saved and reused for consistency between experiments. Images were taken until 100+ macrophages were sampled. To analyze these images, we used a custom MATLAB script. This script uses defined cell size ratios and edge detection to pick out single cells and objects (up to 4 cells clumped together) and measures the average pixel intensity, max pixel intensity, and area of each object. This script thresholds out the background and subtracts this measurement from the average cellular pixel intensities. This script is available on GitHub at https://github.com/gclark304/fluorescent_image_analysis.

Statistical analysis of cellular pixel intensities

Average cellular pixel intensities were used as a proxy for of Aß phagocytosis. At least 100 cells measured per time point were analyzed using the above-described software. All measurements below the background signal were considered below the threshold and removed. The average pixel intensities were then log10 transformed and the interquartile range (IQR) was used to remove outliers. ECHO, Welch's two-sample T-tests, and Hedges' g were used to determine the statistical significance of the differences between the average cellular pixel intensities [42]. We ran a Hedges' g since it is an appropriate statistical analysis to measure effect with samples of varying sample size. A Hedges' g value above 0.2 shows a small effect, above 0.5 shows a medium effect, and above 0.8 shows a large effect; therefore, a large Hedges' g confirms significance whereas a small Hedges' g negates significance. All raw phagocytosis data of cellular pixel intensities are available on Mendeley Data (doi: 10.17632/zrmgjyggmr.1).

ECHO Analysis

ECHO version 4.1 was used to analyze all transcriptome, proteome, PG concentrations, and phagocytosis data that had samples gathered over circadian time [42]. All data were free run with the smooth data and linear detrend data options selected. In order to be considered circadian, the ECHO model must predict a period of 18-30 hours, an AC coefficient of ± 0.15 , and all p-values including BH and BY adjust p-values to be less than 0.05. Transcriptome data is reported in normalized transcripts per million and the proteome data is reported in normalized spectral counts. Transcriptome and Proteome data analyzed in ECHO has an x-axis of 0 to 46 corresponding to the number of samples taken in chronological order, which when

added to 16 equals the post shock time of each sample. In order to calculate zeniths for the transcriptome and proteome data, the hours shifted from the ECHO analysis was added to 16 to get the post shock time, which was then converted to CT time using Keller et al., 2009 [41]. PG level analysis included all four replicates per time point. For the phagocytosis data, the average of the replicates was analyzed at each time point.

Liquid chromatography-tandem mass spectrometry

Using synchronized macrophages (as described above) starting at PS16 every 4 h for 24 h (PS16, PS20, PS24, PS28, PS32, PS36, and PS40), macrophages, in quadruplicate, were washed once with PBS, and removed from the plate using Cell Stripper (Corning 25-056-CI). Macrophages were centrifuged at 400 g for three minutes, the supernatant was aspirated, the cells were resuspended in 250 μ L PBS, and flash frozen. Additionally, at PS16, PS20, PS28, and PS36, spent media from each culture dish was centrifuged at 400 x g for three minutes to remove any particulates and flash frozen. Finally, after macrophage removal, at PS16, PS20, PS28, and PS36, the culture dish was scraped using a sterile rubber policeman, the dish was flushed with 1 ml of PBS, and the resultant sample was flash frozen to sample the ECM.

To analyze total cellular levels of PGs using LC-MS/MS, macrophage pellets were treated with 100 μl BugBuster 10× protein extraction reagent (MilliporeSigma) and transferred into 1 mL microcentrifuge tubes, which were then sonicated at room temperature for 20 min. After that, 300 µl digestion buffer (50 mM ammonium acetate, 2 mM calcium chloride) was added. To analyze total supernatant and ECM levels of PGs using LC-MS/MS, 400 µl of clarified supernatant/ECM scrapings were loaded onto a 3 KDa spin column (Millipore Sigma UFC500396), washed with distilled water, and then the upper solution was aspirated and mixed with 300 µl digestion buffer. In all cases, recombinant heparin lyase I, II, III and chondroitin lyase ABC (10 mU each) (prepared by the Linhardt lab) were added to the 300 µl of digestion buffer and incubated at 37°C overnight. Digestion reactions were terminated by passing the sample through a 3 KDa MWCO spin column to eliminate the lyases. The 3 KDa MWCO spin columns were washed twice with 300 µl distilled water and the filtrate was lyophilized. Lyophilized samples were AMAC-labeled by incubating them at room temperature for 10 min with 10 μl of 0.1 M AMAC in DMSO/acetic acid (17/3,V/V), after which 10 μl of 1 M aqueous NaBH₃CN was added and the mixture was incubated for 1 h at 45°C. The resultant samples were centrifuged at 13,200 rpm for 10 min. Finally, each supernatant was collected and stored in a light resistant container at room temperature until LC-MS/MS analysis.

LC was performed on an Agilent 1200 LC system at 45° C using an Agilent Poroshell 120 ECC18 (2.7 µm, 3.0×50 mm) column. Mobile phase A (MPA) was a 50 mM ammonium acetate aqueous solution, and mobile phase B (MPB) was methanol. The mobile phase passed through the column at a flow rate of $300 \,\mu$ l/min. The gradient was 0– $10 \,\text{min}$, 5–45% B; 10– $10.2 \,\text{min}$, 45–100%B; 10.2– $14 \,\text{min}$, 100%B; 14– $22 \,\text{min}$, 100–5%B. A triple quadrupole mass spectrometry system equipped with an ESI source (Thermo Fisher Scientific, San Jose, CA) was used as a detector. The online MS analysis was in the multiple reaction monitoring (MRM) mode. MS parameters: negative ionization mode with a spray voltage of $3,000 \,\text{V}$, a vaporizer temperature of 300° C, and a capillary temperature of 270° C. The conditions and collision energies for all of the disaccharides MRM transitions are listed in S6 Table. Sample measurements for the cell pellet were normalized in nanograms of PGs per cell (ng/cell) using a CyQUANT Assay to quantify the number of cells used per pellet as described in the Methods. Sample measurements from the ECM and spent media samples were calculated in nanograms per milliliter (ng/ml). All HSPG and CSPG raw data generated from this experiment are available on Mendeley Data (doi: 10.17632/zrmgjyggmr.1).

CyQUANT assay

Due to the varying amount of protein present in a cell over time, we normalized the HSPG and CSPG cell pellet findings to the number of cells present in each sample. The cells were quantified using a CyQUANT Cell Proliferation assay (Invitrogen C7026). This kit was used to lyse 100 μ l of the cells stripped from each plate and stain the nucleic acids with a fluorescently labeled dye (included in kit cited above), which was then read by a plate reader at an excitation wavelength of 480 nm and emission wavelength of 520 nm. The concentration of cells was then back calculated using a standard curve made by measuring known amounts of the primary murine macrophages. This standard curve was constructed per the manufacturer's instructions (Invitrogen C7026 manual). The cells were diluted to a known amount using a BioRad TC20 automated cell counter, lysed, dyed, and read on a Tecan Infinite M1000 Pro plate reader at an excitation wavelength of 480 nm and emission wavelength at 520 nm. The number of cells from each sample was first calculated using the equation of the standard curve (R² = 0.9938) and then multiplied by the dilution factor to calculate the total number of cells in each cell pellet.

Production of heparinases

Heparinases were prepared as has been previously reported [63–65]. All heparinases used were purified away from endotoxins using an Endotoxin Removal Kit from GenScript (L00338) [66].

Supporting information

S1 Fig. The murine circadian clock times macrophage physiology. The macrophage circadian rhythm is imposed by a conserved, core molecular clock that imparts control of key gene and protein expression through a transcription/translation negative feedback loop (TTFL). In murine macrophages, pictured as the blue cell above, the positive arm of the clock, in the core circadian timekeeper (Loop 1), is made up of ARNTL and CLOCK, which binds to the Ebox promoter to turn on the creation of the negative arm protein (PER, CRY), auxiliary loop proteins (NR1D1, DBP, ROR), and clock-controlled genes (ccgs). The negative arm proteins then dimerize in the cytoplasm and are temporally phosphorylated by CK1 (also known as Csnk1a1 in mice), until they migrate back into the nucleus and inhibit their own transcription by inhibiting ARNTL and CLOCK, the negative arm is then ubiquinated and degraded, restarting the cycle. Two auxiliary loops to the circadian clock, Loop 2 and Loop 3, impart further fine-tuning of circadian regulation. In Loop 2, the cycle starts when ROR binds to the ROR promoter sequences to turn on expression of arntl, nfil3, and other ccgs. This loop is inhibited when the positive arm activates transcription of NR1D1, which inhibits transcription in Loop 2. Loop 3 is activated via the DBP binding to the D-box promoter and turns on expression of PER and CCGs. This expression is in turn inhibited by the expression of NFIL3 from Loop 2. The surrounding gene expression graphs show the timing of expression of key clock proteins in Post Shock (PS) time and Circadian Time (CT) using transcriptome data from Collins et al., 2020 [S1] [28]. The murine clock pathway was adapted from Curtis et al., 2014 [S2] [124].(TIF)

S2 Fig. Schematic of the macrophage phagocytosis assay protocol. Our procedure began with the extraction of bone marrow monocytes from PER2::LUC mice. Extracted bone marrow monocytes were treated with mCSF with fresh media (10% FBS) added every 3 days and these bone marrow derived macrophages were grown to confluency. After seven days,

macrophages were transferred to media without serum (0%FBS) for 24 hours before being transferred to serum shock media (50% FBS) for 2 hours, in order to synchronize their clocks. Synchronized macrophages were transferred into fresh media (10% FBS) and, starting at 16 hours post shock (PS 16), samples were treated in triplicate with A β (for 2 hours) every four hours for 24 hours. Macrophages were then harvested, fixed using formalin, and imaged using fluorescence microscopy. PS hours as represented in yellow for the active and grey for the inactive phase of the mice as reported previously [S1]. (TIF)

S3 Fig. Aβ42 phagocytosis oscillates with a circadian period. A) The log of mean cell fluorescence of Aβ42 phagocytosis in PER2::LUC cells (purple circles), and in PER1^{-/-}PER2^{-/-} knockout cells (brown squares) plotted over time. Error bars represent the standard deviation. B) Violin plot of Aβ42 phagocytosis in PER1^{-/-}PER2^{-/-} knockout cells represented in logged mean cell fluorescence values plotted against post shock (PS) and circadian time (CT). Grey dots represent a single cell measurement, brown violin plot lines represent the range of the data, and red diamonds indicate the mean measurement of each time point. CT is in reference to the comparison of PER2 expression from Keller et al., 2009 [S3] [41] compared to PER2 expression from our cells. All data shown was performed in triplicate. (TIF)

S4 Fig. Schematic of the quantification of PGs in BMDMs. (A) BMDMs were collected at PS 16, 20, 24, 28, 32, and 36, in quadruplicate. Spent media from these cell pellets was collected at PS 16, 20, 28, and 36, in triplicate. Concurrently, ECM samples were collected in duplicate at post shock times 16, 20, 28, and 36. (B) The above samples were analyzed by LC-MS/MS and normalized using data from a CyQUANT assay that calculated total cellular DNA by UV-VIS spectroscopy and an interpolated standard curve (standard curve in inset from actual macrophage data). (TIF)

S5 Fig. HSPG and CSPG levels oscillate over circadian time in murine macrophages. (A) The level of each HSPG sulfation type in macrophage cells (n=4) plotted against PS and CT time. (B) The level of each HSPG sulfation type in macrophage ECM scrapings (n=2) plotted against PS and CT time. (C) The level of each HSPG sulfation type in macrophage spent media cultures (n=3) plotted against PS and CT time. (D) The level of each CSPG sulfation type in macrophage cells (n=4) plotted against PS and CT time. (E) The level of each CSPG sulfation type in macrophage ECM scrapings (n=2) plotted against PS and CT time. (F) The level of each CSPG sulfation type in macrophage spent media cultures (n=3) plotted against PS and CT time. (n=3) plotted against PS and CT time.

S6 Fig. Heparinases I and III differentially disrupt the phagocytosis of A β 42. Violin plot of A β 42 phagocytosis in the presence of A) Heparinase I and B) Heparinase III represented in logged mean cell fluorescence values plotted against PS and CT. Grey dots represent a single cell measurement, A) red and B) maroon violin plot lines represent the range of the data, and red diamonds indicate the mean measurement of each time point. CT is in reference to the comparison of PER2 expression from Keller et al., 2009 [S3] [41] compare to PER2 expression from our cells. C) Phagocytosis of A β 42 when heparinases I, II, and III are added at decreasing concentrations (shown in key), represented in the log of the mean cell fluorescence over PS and CT time. (TIF)

S1 Table. ECHO analysis of the Aβ42 phagocytosis assays.

(XLSX)

S2 Table. ECHO analysis of the transcripts and proteins in the PG pathway.

(XLSX)

S3 Table. ECHO analysis of lipid receptors and cell cycle proteins.

(XLSX)

S4 Table. ECHO analysis of the HSPG and CSPG levels in the macrophage cell pellet.

(XLSX)

S5 Table. Heparinase concentrations and activities.

(XLSX)

S6 Table. Conditions and collision energies for the disaccharide MRM transitions.

(XLSX)

Acknowledgments

We would like to acknowledge Emily Collins for her transcriptome and proteome datasets, Lufeng Yu for performing heparinase activity assays, Ke Xia for providing editing on the LC-MS/MS section, and the PER1^{-/-}/PER2^{-/-} knockout mice shared by the labs of Jay Dunlap and Jennifer Loros. Additionally, we would like to acknowledge the Analytical Biochemistry Core at RPI, Sergey Pryshchep of the Microscopy core at RPI for his training and guidance, and Antigone McKenna and the BioResearch core staff at RPI for their excellent care of our mouse lines. We would like to thank BioRender.com for support in figure creation.

Author Contributions

Conceptualization: Gretchen T. Clark, Chunyu Wang, Robert J. Linhardt, Jennifer M. Hurley.

Data curation: Gretchen T. Clark, Yanlei Yu, Cooper A. Urban, Fuming Zhang.

Formal analysis: Gretchen T. Clark, Jennifer M. Hurley.

Funding acquisition: Robert J. Linhardt, Jennifer M. Hurley.

Investigation: Gretchen T. Clark, Yanlei Yu, Chunyu Wang, Fuming Zhang, Robert J. Linhardt, Jennifer M. Hurley.

narat, jenniner ivi. Trancy.

Methodology: Gretchen T. Clark, Fuming Zhang.

Project administration: Jennifer M. Hurley.

Resources: Guo Fu, Jennifer M. Hurley.

Software: Gretchen T. Clark, Guo Fu.

Supervision: Fuming Zhang, Robert J. Linhardt, Jennifer M. Hurley.

Validation: Cooper A. Urban.

Visualization: Gretchen T. Clark, Cooper A. Urban.

Writing – original draft: Gretchen T. Clark, Jennifer M. Hurley.

Writing – review & editing: Gretchen T. Clark, Chunyu Wang, Robert J. Linhardt, Jennifer

M. Hurley.

References

- 2019 Alzheimer's disease facts and figures. Alzheimer's Dement [Internet]. 2019 Mar 1; 15(3):321–87. Available from: https://doi.org/10.1016/j.jalz.2019.01.010.
- El-Hayek YH, Wiley RE, Khoury CP, Daya RP, Ballard C, Evans AR, et al. Tip of the iceberg: Assessing the global socioeconomic costs of Alzheimer's Disease and related dementias and strategic implications for stakeholders. J Alzheimer's Dis [Internet]. 2019 Jul 23; 70(2):323–41. Available from: https://www.medra.org/servlet/aliasResolver?alias=iospress&doi=10.3233/JAD-190426 PMID: 31256142
- 3. Prince M. A, Wimo A, Guerchet M, Gemma-Claire Ali M, Wu Y-T, Prina M, et al. World Alzheimer report 2015 the global impact of dementia an analysis of prevalence, incidence, cost and trends [Internet]. 2015. www.alz.co.uk/worldreport2015corrections.
- 4. Barage SH, Sonawane KD. Amyloid cascade hypothesis: Pathogenesis and therapeutic strategies in Alzheimer's disease. Neuropeptides [Internet]. 2015 Aug 1; 52:1–18. Available from: https:// linkinghub.elsevier.com/retrieve/pii/S0143417915000657 PMID: 26149638
- Uddin MS, Kabir MT, Rahman MS, Behl T, Jeandet P, Ashraf GM, et al. Revisiting the amyloid cascade hypothesis: From anti-aβ therapeutics to auspicious new ways for alzheimer's disease. Int J Mol Sci [Internet]. 2020 Aug 2; 21(16):1–33. Available from: /pmc/articles/PMC7461598/. https://doi.org/ 10.3390/ijms21165858 PMID: 32824102
- 6. Huang Y. Effects of Age and Amyloid Deposition on Aβ Dynamics in the Human Central Nervous System. Arch Neurol [Internet]. 2012 Jan 1; 69(1):51. Available from: http://archneur.jamanetwork.com/article.aspx?doi=10.1001/archneurol.2011.235 PMID: 21911660
- Zhang R, Miller RG, Madison C, Jin X, Honrada R, Harris W, et al. Systemic immune system alterations in early stages of Alzheimer's disease. J Neuroimmunol [Internet]. 2013 Mar; 256(1–2):38–42.
 Available from: https://linkinghub.elsevier.com/retrieve/pii/S0165572813000040 PMID: 23380586
- Musiek ES, Xiong DD, Holtzman DM. Sleep, circadian rhythms, and the pathogenesis of Alzheimer Disease. Exp & Mol Med [Internet]. 2015 Mar 13; 47:e148. Available from: https://doi.org/https://doi.org/https://doi.org/10.1038/emm.2014.121 PMID: 25766617
- Musiek ES, Bhimasani M, Zangrilli MA, Morris JC, Holtzman DM, Ju Y-ES. Circadian Rest-Activity Pattern Changes in Aging and Preclinical Alzheimer Disease. JAMA Neurol [Internet]. 2018 May 1; 75 (5):582. Available from: http://archneur.jamanetwork.com/article.aspx?doi=10.1001/jamaneurol.2017.4719 PMID: 29379963
- Sadeghmousavi S, Eskian M, Rahmani F, Rezaei N. The effect of insomnia on development of Alzheimer's disease [Internet]. Vol. 17, Journal of Neuroinflammation. BioMed Central Ltd; 2020. /pmc/articles/PMC7542374/. https://doi.org/10.1186/s12974-020-01960-9 PMID: 33023629
- Fiala M, Zhang L, Gan X, Sherry B, Taub D, Graves MC, et al. Amyloid-β Induces Chemokine Secretion and Monocyte Migration across a Human Blood-Brain Barrier Model. Mol Med [Internet]. 1998 Jul 1; 4(7):480–9. Available from: https://molmed.biomedcentral.com/articles/10.1007/BF03401753. PMID: 9713826
- Simard AR, Rivest S. Neuroprotective properties of the innate immune system and bone marrow stem cells in Alzheimer's disease [Internet]. Vol. 11, Molecular Psychiatry. Mol Psychiatry; 2006. p. 327– 35. https://pubmed.ncbi.nlm.nih.gov/16491130/.
- 13. Zhang K, Tian L, Liu L, Feng Y, Dong Y Bin, Li B, et al. CXCL1 contributes to β-amyloid-induced transendothelial migration of monocytes in Alzheimer's Disease. PLoS One [Internet]. 2013 Aug 14; 8(8): e72744. Available from: http://www.ncbi.nlm.nih.gov/pubmed/23967336 PMID: 23967336
- 14. Mildner A, Schlevogt B, Kierdorf K, Bottcher C, Erny D, Kummer MP, et al. Distinct and Non-Redundant Roles of Microglia and Myeloid Subsets in Mouse Models of Alzheimer's Disease. J Neurosci [Internet]. 2011 Aug 3; 31(31):11159–71. Available from: https://www.jneurosci.org/lookup/doi/10.1523/JNEUROSCI.6209-10.2011 PMID: 21813677
- Möhle L, Israel N, Paarmann K, Krohn M, Pietkiewicz S, Müller A, et al. Chronic Toxoplasma gondii infection enhances β-amyloid phagocytosis and clearance by recruited monocytes. Acta Neuropathol Commun [Internet]. 2016 Mar 16; 4:25. Available from: https://link.springer.com/articles/10.1186/s40478-016-0293-8 PMID: 26984535
- Yang HS, Onos KD, Choi K, Keezer KJ, Skelly DA, Carter GW, et al. Natural genetic variation determines microglia heterogeneity in wild-derived mouse models of Alzheimer's disease. Cell Rep [Internet]. 2021 Feb 9; 34(6):108739. Available from: https://doi.org/10.1016/j.celrep.2021.108739 PMID: 33567283
- 17. Hickman SE, Allison EK, Khoury J El. Microglial dysfunction and defective-amyloid clearance pathways in aging Alzheimer's Disease mice. Neurobiol Dis [Internet]. 2008; 28(33):8354–60. Available from: www.jneurosci.org PMID: 18701698

- Grammas P. Inflammatory factors are elevated in brain microvessels in Alzheimer's disease. Neurobiol Aging [Internet]. 2001 Dec 1; 22(6):837–42. Available from: https://linkinghub.elsevier.com/ retrieve/pii/S0197458001002767 PMID: 11754990
- Zaghi J, Goldenson B, Inayathullah M, Lossinsky AS, Masoumi A, Avagyan H, et al. Alzheimer disease macrophages shuttle amyloid-beta from neurons to vessels, contributing to amyloid angiopathy. Acta Neuropathol [Internet]. 2009 Feb 13; 117(2):111–24. Available from: http://link.springer.com/10.1007/s00401-008-0481-0 PMID: 19139910
- Marsh SE, Abud EM, Lakatos A, Karimzadeh A, Yeung ST, Davtyan H, et al. The adaptive immune system restrains Alzheimer's disease pathogenesis by modulating microglial function. Proc Natl Acad Sci [Internet]. 2016 Mar 1; 113(9):E1316–25. Available from: http://www.pnas.org/lookup/doi/10.1073/pnas.1525466113 PMID: 26884167
- 21. Jevtic S, Sengar AS, Salter MW, McLaurin JA. The role of the immune system in Alzheimer disease: Etiology and treatment [Internet]. Vol. 40, Ageing Research Reviews. Elsevier Ireland Ltd; 2017. p. 84–94. http://www.ncbi.nlm.nih.gov/pubmed/28941639.
- 22. Le Page A, Dupuis G, Frost EH, Larbi A, Pawelec G, Witkowski JM, et al. Role of the peripheral innate immune system in the development of Alzheimer's disease. Exp Gerontol [Internet]. 2018 Jul; 107:59–66. Available from: https://linkinghub.elsevier.com/retrieve/pii/S0531556517305417 PMID: 29275160
- Jairani PS, Aswathy PM, Krishnan D, Menon RN, Verghese J, Mathuranath PS, et al. Apolipoprotein E polymorphism and oxidative stress in peripheral blood-derived macrophage-mediated amyloid-beta phagocytosis in Alzheimer's Disease patients. Cell Mol Neurobiol [Internet]. 2019; 39(3):355–69. Available from: https://doi.org/10.1007/s10571-019-00651-1 PMID: 30694418
- Brás JP, Bravo J, Freitas J, Barbosa MA, Santos SG, Summavielle T, et al. TNF-alpha-induced microglia activation requires miR-342: impact on NF-kB signaling and neurotoxicity. Cell Death Dis [Internet]. 2020 Jun 2; 11(6):415. Available from: http://www.nature.com/articles/s41419-020-2626-6 PMID: 32488063
- 25. Li S, Hayden EY, Garcia VJ, Fuchs D-T, Sheyn J, Daley DA, et al. Activated Bone Marrow-Derived Macrophages Eradicate Alzheimer's-Related Aβ42 Oligomers and Protect Synapses. Front Immunol [Internet]. 2020 Jan 31; 11. Available from: https://www.frontiersin.org/article/10.3389/fimmu.2020.
- Labrecque N, Cermakian N. Circadian clocks in the immune system [Internet]. Vol. 30, Journal of Biological Rhythms. SAGE Publications Inc.; 2015. p. 277–90. http://www.ncbi.nlm.nih.gov/pubmed/25900041.
- Hergenhan S, Holtkamp S, Scheiermann C. Molecular interactions between components of the circadian clock and the immune system. J Mol Biol [Internet]. 2020; 432(12):3700–13. Available from: http://www.sciencedirect.com/science/article/pii/S0022283620300280 PMID: 31931006
- Collins EJ, Cervantes-Silva MP, Timmons GA, O'Siorain JR, Curtis AM, Hurley JM. Post-transcriptional circadian regulation in macrophages organizes temporally distinct immunometabolic states.
 Genome Res [Internet]. 2021 Feb 1; 31(2):171–85. Available from: https://genome.cshlp.org/content/31/2/171.full PMID: 33436377
- O'Callaghan P, Sandwall E, Li, Yu H, Ravid R, Guan Z-Z, et al. Heparan sulfate accumulation with Abeta deposits in Alzheimer's disease and Tg2576 mice is contributed by glial cells. Brain Pathol [Internet]. 2008/04/11. 2008 Oct; 18(4):548–61. Available from: https://www.ncbi.nlm.nih.gov/pubmed/18422760 PMID: 18422760
- 30. Liu C-C, Zhao N, Yamaguchi Y, Cirrito JR, Kanekiyo T, Holtzman DM, et al. Neuronal heparan sulfates promote amyloid pathology by modulating brain amyloid-β clearance and aggregation in Alzheimer's disease. Sci Transl Med [Internet]. 2016 Mar 30; 8(332). Available from: https://www.ncbi.nlm.nih.gov/pubmed/27030596 PMID: 27030596
- 31. Fraser PE, Darabie AA, McLaurin JA. Amyloid-β interactions with chondroitin sulfate-derived monosaccharides and disaccharides: Implications for drug development. J Biol Chem [Internet]. 2001 Mar 2; 276(9):6412–9. Available from: https://pubmed.ncbi.nlm.nih.gov/11106653/ PMID: 11106653
- **32.** Esko JD, Selleck SB. ORDER OUT OF CHAOS: Assembly of Ligand Binding Sites in Heparan Sulfate 1. 2002; 71:435–71. Available from: www.annualreviews.org.
- Sandwall E, O'Callaghan P, Zhang X, Lindahl U, Lannfelt L, Li J-P. Heparan sulfate mediates amyloidbeta internalization and cytotoxicity. Glycobiology [Internet]. 2010 May 1; 20(5):533–41. Available from: https://doi.org/10.1093/glycob/cwp205 PMID: 20053627
- 34. Zhang X, Li J-P. Heparan sulfate proteoglycans in amyloidosis. In: Zhang LBT, editor. Glycosamino-glycans in Development, Health and Disease [Internet]. Academic Press; 2010. p. 309–34. http://www.sciencedirect.com/science/article/pii/S1877117310930135.

- 35. Zhang X, Wang B, O'Callaghan P, Hjertström E, Jia J, Gong F, et al. Heparanase overexpression impairs inflammatory response and macrophage-mediated clearance of amyloid-β in murine brain. Acta Neuropathol [Internet]. 2012 Oct; 124(4):465–78. Available from: https://pubmed.ncbi.nlm.nih.gov/22692572/ PMID: 22692572
- Marques F, Sousa JC, Sousa N, Palha JA. Blood-brain-barriers in aging and in Alzheimer's disease [Internet]. Vol. 8, Molecular Neurodegeneration. BioMed Central; 2013. p. 1–9. https://link.springer.com/articles/10.1186/1750-1326-8-38.
- 37. Trouplin V, Boucherit N, Gorvel L, Conti F, Mottola G, Ghigo E. Bone marrow-derived macrophage production. J Vis Exp [Internet]. 2013;(81):50966. Available from: /pmc/articles/PMC3991821/. https://doi.org/10.3791/50966 PMID: 24300014
- 38. Franco R, Fernández-Suárez D. Alternatively activated microglia and macrophages in the central nervous system [Internet]. Vol. 131, Progress in Neurobiology. Elsevier Ltd; 2015. p. 65–86. https://doi.org/http%3A//dx.doi.org/10.1016/j.pneurobio.2015.05.003 PMID: 26067058
- **39.** Zhang X, Goncalves R, Mosser DM. The isolation and characterization of murine macrophages [Internet]. Vol. Chapter 14, Current Protocols in Immunology. Curr Protoc Immunol; 2008. https://pubmed.ncbi.nlm.nih.gov/19016445/.
- 40. Yoo S-H, Yamazaki S, Lowrey PL, Shimomura K, Ko CH, Buhr ED, et al. PERIOD2::LUCIFERASE real-time reporting of circadian dynamics reveals persistent circadian oscillations in mouse peripheral tissues. Proc Natl Acad Sci [Internet]. 2004 Apr 13; 101(15):5339–46. Available from: http://www.pnas.org/cgi/doi/10.1073/pnas.0308709101 PMID: 14963227
- Keller M, Mazuch J, Abraham U, Eom GD, Herzog ED, Volk H-D, et al. A circadian clock in macrophages controls inflammatory immune responses. Proc Natl Acad Sci [Internet]. 2009 Dec 15; 106 (50):21407 LP–21412. Available from: http://www.pnas.org/content/106/50/21407.abstract PMID: 19955445
- De los Santos H, Collins EJ, Mann C, Sagan AW, Jankowski MS, Bennett KP, et al. ECHO: an application for detection and analysis of oscillators identifies metabolic regulation on genome-wide circadian output. Bioinformatics [Internet]. 2020 Feb 1; 36(3):773–81. Available from: https://academic.oup.com/bioinformatics/article/36/3/773/5544107 PMID: 31384918
- 43. Castellano JM, Deane R, Gottesdiener AJ, Verghese PB, Stewart FR, West T, et al. Low-density lipoprotein receptor overexpression enhances the rate of brain-to-blood Aβ clearance in a mouse model of β-amyloidosis. Proc Natl Acad Sci U S A [Internet]. 2012 Sep 18; 109(38):15502–7. Available from: https://www.pnas.org/content/109/38/15502 PMID: 22927427
- 44. Hyman BT, Strickland D, Rebeck GW. Role of the low-density lipoprotein receptor-related protein in β-amyloid metabolism and Alzheimer disease. Arch Neurol [Internet]. 2000 May 1; 57(5):646–50. Available from: https://jamanetwork.com/ PMID: 10815129
- 45. Mi H, Ebert D, Muruganujan A, Mills C, Albou L-P, Mushayamaha T, et al. PANTHER version 16: a revised family classification, tree-based classification tool, enhancer regions and extensive API. Nucleic Acids Res [Internet]. 2021 Jan 8; 49(D1):D394–403. Available from: https://academic.oup.com/nar/article/49/D1/D394/6027812 PMID: 33290554
- 46. Ariga T, Miyatake T, Yu RK. Role of proteoglycans and glycosaminoglycans in the pathogenesis of Alzheimer's disease and related disorders: Amyloidogenesis and therapeutic strategies—A review. J Neurosci Res [Internet]. 2010 Aug 15; 88(11):2303–15. Available from: https://pubmed.ncbi.nlm.nih. gov/20623617/ PMID: 20623617
- Wu F, Zhou C, Zhou D, Ou S, Liu Z, Huang H. Immune-enhancing activities of chondroitin sulfate in murine macrophage RAW 264.7 cells. Carbohydr Polym [Internet]. 2018 Oct 15; 198:611–9. Available from: https://linkinghub.elsevier.com/retrieve/pii/S0144861718307252 PMID: 30093041
- 48. Snow AD, Sekiguchi R, Nochlin D, Fraser P, Kimata K, Mizutani A, et al. An important role of heparan sulfate proteoglycan (perlecan) in a model system for the deposition and persistence of fibrillar aβ-amyloid in rat brain. Neuron [Internet]. 1994 Jan 1; 12(1):219–34. Available from: https://linkinghub.elsevier.com/retrieve/pii/0896627394901651 PMID: 8292358
- 49. Snow AD, Kinsella MG, Parks E, Sekiguchi RT, Miller JD, Kimata K, et al. Differential binding of vascular cell-derived proteoglycans (perlecan, biglycan, decorin, and versican) to the beta-amyloid protein of Alzhiemer's Disease [Internet]. Archives of Biochemistry and Biophysics; 1995. p. 84–95. https://pubmed.ncbi.nlm.nih.gov/7793988/.
- Castillo GM, Lukito W, Wight TN, Snow AD. The sulfate moieties of glycosaminoglycans are critical for the enhancement of β-amyloid protein fibril formation. J Neurochem [Internet]. 1999 Apr 1; 72
 (4):1681–7. Available from: https://onlinelibrary.wiley.com/doi/full/10.1046/j.1471-4159.1999.721681.
 × PMID: 10098877
- Li J-P, Galvis MLE, Gong F, Zhang X, Zcharia E, Metzger S, et al. In vivo fragmentation of heparan sulfate by heparanase overexpression renders mice resistant to amyloid protein A amyloidosis. Proc Natl

- Acad Sci [Internet]. 2005 May 3; 102(18):6473–7. Available from: https://www.pnas.org/content/102/18/6473 PMID: 15843464
- 52. Bruinsma IB, te Riet L, Gevers T, ten Dam GB, van Kuppevelt TH, David G, et al. Sulfation of heparan sulfate associated with amyloid-β plaques in patients with Alzheimer's disease. Acta Neuropathol [Internet]. 2010 Feb 28; 119(2):211–20. Available from: http://link.springer.com/10.1007/s00401-009-0577-1 PMID: 19636575
- 53. Wall JS, Richey T, Stuckey A, Donnell R, Oosterhof A, van Kuppevelt TH, et al. SPECT imaging of peripheral amyloid in mice by targeting hyper-sulfated heparan sulfate proteoglycans with specific scFv antibodies. Nucl Med Biol [Internet]. 2012; 39(1):65–75. Available from: http://dx.doi.org/10. 1016/j.nucmedbio.2011.06.007 PMID: 21958847
- Maeda N. Proteoglycans and neuronal migration in the cerebral cortex during development and disease. Front Neurosci [Internet]. 2015 Mar 23; 9:98. Available from: http://www.frontiersin.org/Neurogenesis/10.3389/fnins.2015.00098/abstract PMID: 25852466
- Kreuger J, Kjellén L. Heparan sulfate biosynthesis: regulation and variability. J Histochem Cytochem [Internet]. 2012; 60(12):898–907. Available from: https://pubmed.ncbi.nlm.nih.gov/23042481/PMID:23042481
- 56. Ly M, Leach FE, Laremore TN, Toida T, Amster IJ, Linhardt RJ. The proteoglycan bikunin has a defined sequence. Nat Chem Biol [Internet]. 2011; 7(11):827–33. Available from: /pmc/articles/PMC3197799/?report=abstract. https://doi.org/10.1038/nchembio.673 PMID: 21983600
- 57. Eppig JT. Mouse genome informatics (MGI) resource: Genetic, genomic, and biological knowledge-base for the laboratory mouse. ILAR J [Internet]. 2017 Jul 1; 58(1):17–41. Available from: https://academic.oup.com/ilarjournal/article/58/1/17/3867191 PMID: 28838066
- Castedo M, Perfettini J-L, Roumier T, Yakushijin K, Horne D, Medema R, et al. The cell cycle check-point kinase Chk2 is a negative regulator of mitotic catastrophe. Oncogene [Internet]. 2004 May 29; 23(25):4353–61. Available from: http://www.nature.com/articles/1207573 PMID: 15048074
- Rankin S, Ayad NG, Kirschner MW. Sororin, a substrate of the anaphase- promoting complex, is required for sister chromatid cohesion in vertebrates. Mol Cell [Internet]. 2005 Apr 15; 18(2):185–200. Available from: https://pubmed.ncbi.nlm.nih.gov/15837422/ PMID: 15837422
- 60. Hanse EA, Nelsen CJ, Goggin MM, Anttila CK, Mullany LK, Berthet C, et al. Cdk2 plays a critical role in hepatocyte cell cycle progression and survival in the setting of cyclin D1 expression in vivo. Cell Cycle [Internet]. 2009 Sep 28; 8(17):2802–9. Available from: http://www.tandfonline.com/doi/abs/10.4161/cc.8.17.9465 PMID: 19652536
- 61. Ughy B, Schmidthoffer I, Szilak L. Heparan sulfate proteoglycan (HSPG) can take part in cell division: inside and outside. Cell Mol Life Sci [Internet]. 2019 Mar 15; 76(5):865–71. Available from: https://doi.org/10.1007/s00018-018-2964-z PMID: 30465083
- 62. Hong CI, Zamborszky J, Baek M, Labiscsak L, Ju K, Lee H, et al. Circadian rhythms synchronize mitosis in Neurospora crassa. Proc Natl Acad Sci [Internet]. 2014 Jan 28; 111(4):1397–402. Available from: http://www.pnas.org/cgi/doi/10.1073/pnas.1319399111 PMID: 24474764
- 63. Yang VC, Linhardt RJ, Bernstein H, Cooney CL, Langer R. Purification and characterization of heparinase from Flavobacterium heparinum. J Biol Chem [Internet]. 1985 Feb; 260(3):1849–57. Available from: https://linkinghub.elsevier.com/retrieve/pii/S0021925818896715. PMID: 3968088
- 64. Ernst S, Venkataraman G, Winkler S, Godavarti R, Langer R, Cooney CL, et al. Expression in Escherichia coli, purification and characterization of heparinase I from Flavobacterium heparinum. Biochem J [Internet]. 1996 Apr 15; 315(2):589–97. Available from: https://pubmed.ncbi.nlm.nih.gov/8615834/
 PMID: 8615834
- 65. Godavarti R, Davis M, Venkataraman G, Cooney C, Langer R, Sasisekharan R. Heparinase III from Flavobacterium heparinum: cloning and recombinant expression in Escherichia coli. Biochem Biophys Res Commun [Internet]. 1996 Aug 23; 225(3):751–8. Available from: https://linkinghub.elsevier.com/ retrieve/pii/S0006291X96912462 PMID: 8780685
- 66. Chen N, Wan X-L, Huang C-X, Wang W-M, Liu H, Wang H-L. Study on the immune response to recombinant Hsp70 protein from Megalobrama amblycephala. Immunobiology [Internet]. 2014 Nov 1; 219(11):850–8. Available from: https://linkinghub.elsevier.com/retrieve/pii/S0171298514001259
 PMID: 25113416
- Scholefield Z, Yates EA, Wayne G, Amour A, McDowell W, Turnbull JE. Heparan sulfate regulates amyloid precursor protein processing by BACE1, the Alzheimer's β-secretase. J Cell Biol [Internet]. 2003 Oct 13; 163(1):97–107. Available from: http://www.jcb.org/cgi/doi/10.1083/jcb.200303059 PMID: 14530380
- **68.** Silva ME, Dietrich CP. Structure of heparin. Characterization of the products formed from heparin by the action of a heparinase and a heparitinase from Flavobacterium heparinum. J Biol Chem [Internet].

- 1975 Sep 10; 250(17):6841–6. Available from: https://linkinghub.elsevier.com/retrieve/pii/S0021925819410089. PMID: 1158884
- **69.** Linhardt RJ, Grant A, Cooney CL, Langer R. Differential anticoagulant activity of heparin fragments prepared using microbial heparinase. J Biol Chem [Internet]. 1982 Jul 10; 257(13):7310–3. Available from: http://www.jbc.org/article/S0021925818343771/fulltext. PMID: 7085627
- 70. Hausser H, Kresse H. Decorin endocytosis: Structural features of heparin and heparan sulphate oligosaccharides interfering with receptor binding and endocytosis. Biochem J [Internet]. 1999 Dec 15; 344(3):827–35. Available from: /pmc/articles/PMC1220705/?report=abstract. PMID: 10585870
- van Horssen J, Wesseling P, van den Heuvel LP, de Waal RM, Verbeek MM. Heparan sulphate proteoglycans in Alzheimer's disease and amyloid-related disorders. Lancet Neurol [Internet]. 2003 Aug 1; 2(8):482–92. Available from: https://linkinghub.elsevier.com/retrieve/pii/S1474442203004848
 PMID: 12878436
- Fromm J, Hileman R, Caldwell E, Weiler J, Linhardt R. Pattern and spacing of basic amino acids in heparin binding sites. Arch Biochem Biophys [Internet]. 1997 Jul 1; 343(1):92–100. Available from: https://pubmed.ncbi.nlm.nih.gov/9210650/ PMID: 9210650
- 73. Iannuzzi C, Irace G, Sirangelo I. The effect of glycosaminoglycans (GAGs) on amyloid aggregation and toxicity. Molecules [Internet]. 2015 Feb 2; 20(2):2510–28. Available from: https://www.mdpi.com/1420-3049/20/2/2510/htm PMID: 25648594
- 74. Fromm JR, Hileman RE, Caldwell EEO, Weiler JM, Linhardt RJ. Differences in the interaction of heparin with arginine and lysine and the importance of these basic amino acids in the binding of heparin to acidic fibroblast growth factor. Arch Biochem Biophys [Internet]. 1995 Nov 10; 323(2):279–87. Available from: https://pubmed.ncbi.nlm.nih.gov/7487089/ PMID: 7487089
- 75. Caldwell EEO, Nadkarni VD, Fromm JR, Linhardt RJ, Weiler JM. Importance of specific amino acids in protein binding sites for heparin and heparan sulfate. Int J Biochem Cell Biol [Internet]. 1996; 28 (2):203–16. Available from: https://pubmed.ncbi.nlm.nih.gov/8729007/ PMID: 8729007
- Capila I, Linhardt RJ. Heparin—Protein interactions. Angew Chem Int Ed Engl [Internet]. 2002 Feb 1; 41(3):390–412. Available from: https://pubmed.ncbi.nlm.nih.gov/12491369/ PMID: 12491369
- 77. Nguyen K, Rabenstein DL. Interaction of the heparinbBinding consensus sequence of β-amyloid peptides with heparin and heparin-derived oligosaccharides. J Phys Chem B [Internet]. 2016 Mar 17; 120 (9):2187–97. Available from: https://pubmed.ncbi.nlm.nih.gov/26872053/ PMID: 26872053
- Cardin AD, Weintraub HJ. Molecular modeling of protein-glycosaminoglycan interactions. Arterioscler An Off J Am Hear Assoc Inc [Internet]. 1989; 9(1):21–32. Available from: https://www.ahajournals.org/doi/abs/10.1161/01.ATV.9.1.21 PMID: 2463827
- 79. Madine J, Pandya MJ, Hicks MR, Rodger A, Yates EA, Radford SE, et al. Site-specific identification of an Aβ fibril–heparin interaction site by using solid-state NMR spectroscopy. Angew Chemie [Internet]. 2012 Dec 21; 124(52):13317–20. Available from: https://onlinelibrary.wiley.com/doi/full/10.1002/ange. 201204459 PMID: 23161730
- 80. Fraser PE, Nguyen JT, Chin DT, Kirschner DA. Effects of sulfate ions on Alzheimer β/A4 peptide assemblies: Implications for amyloid fibril-proteoglycan interactions. J Neurochem [Internet]. 1992 Oct; 59(4):1531–40. Available from: http://doi.wiley.com/10.1111/j.1471-4159.1992.tb08470.x PMID: 1402902
- 81. McLaurin J, Franklin T, Zhang X, Deng J, Fraser PE. Interactions of Alzheimer amyloid-β peptides with glycosaminoglycans. Eur J Biochem [Internet]. 1999 Dec 15; 266(3):1101–10. Available from: http://doi.wiley.com/10.1046/j.1432-1327.1999.00957.x PMID: 10583407
- McLaurin J, Fraser PE. Effect of amino-acid substitutions on Alzheimer's amyloid-beta peptide-glycosaminoglycan interactions. Eur J Biochem [Internet]. 2000; 267(21):6353–61. Available from: https:// pubmed.ncbi.nlm.nih.gov/11029577/ PMID: 11029577
- 83. Calamai M, Kumita JR, Mifsud J, Parrini C, Ramazzotti M, Ramponi G, et al. Nature and significance of the interactions between amyloid fibrils and biological polyelectrolytes. Biochemistry [Internet]. 2006 Oct 24; 45(42):12806–15. Available from: https://pubs.acs.org/doi/full/10.1021/bi0610653 PMID: 17042499
- **84.** Zhang GL, Zhang X, Wang XM, Li JP. Towards understanding the roles of heparan sulfate proteoglycans in Alzheimer's Disease. Biomed Res Int [Internet]. 2014; 2014. Available from: https://pubmed.ncbi.nlm.nih.gov/25157361/ PMID: 25157361
- **85.** Giulian D, Haverkamp LJ, Yu JH, Karshin W, Tom D, Li J, et al. Specific domains of b-Amyloid from Alzheimer plaque elicit neuron killing in human microglia. 1996; 16(19):6021–37. Available from: https://pubmed.ncbi.nlm.nih.gov/8815885/.
- **86.** Güntert A, Döbeli H, Bohrmann B. High sensitivity analysis of amyloid-beta peptide composition in amyloid deposits from human and PS2APP mouse brain. Neuroscience [Internet]. 2006 Dec 1;

- 143(2):461–75. Available from: https://www.sciencedirect.com/science/article/pii/S0306452206010839?via%3Dihub PMID: 17008022
- 87. Sarasa M, Pesini P. Natural non-trasgenic animal models for research in Alzheimers Disease. Curr Alzheimer Res [Internet]. 2009 Mar 6; 6(2):171–8. Available from:/pmc/articles/PMC2825666/. https://doi.org/10.2174/156720509787602834 PMID: 19355852
- 88. Edrey YH, Medina DX, Gaczynska M, Osmulski PA, Oddo S, Caccamo A, et al. Amyloid beta and the longest-lived rodent: The naked mole-rat as a model for natural protection from Alzheimer's Disease. Neurobiol Aging [Internet]. 2013 Oct 1; 34(10):2352–60. Available from: https://pubmed.ncbi.nlm.nih.gov/23618870/PMID: 23618870
- 89. Lindahl B, Westling C, Giménez-Gallego G, Lindahl U, Salmivirta M. Common binding sites for β-amy-loid fibrils and fibroblast growth factor-2 in heparan sulfate from human cerebral cortex. J Biol Chem [Internet]. 1999 Oct 22; 274(43):30631–5. Available from: https://pubmed.ncbi.nlm.nih.gov/10521448/
 PMID: 10521448
- 90. Gu L, Guo Z. Alzheimer's Aβ42 and Aβ40 peptides form interlaced amyloid fibrils. J Neurochem [Internet]. 2013 Aug 1; 126(3):305–11. Available from: http://doi.wiley.com/10.1111/jnc.12202 PMID: 23406382
- 91. Wesén E, Gallud A, Paul A, Lindberg DJ, Malmberg P, Esbjörner EK. Cell surface proteoglycan-mediated uptake and accumulation of the Alzheimer's disease peptide Aβ(1–42). Biochim Biophys Acta—Biomembr [Internet]. 2018 Nov 1; 1860(11):2204–14. Available from: https://doi.org/10.1016/j.bbamem.2018.08.010 PMID: 30409516
- 92. Rodriguez RA, Chen LY, Plascencia-Villa G, Perry G. Elongation affinity, activation barrier, and stability of Aβ42 oligomers/fibrils in physiological saline. Biochem Biophys Res Commun [Internet]. 2017 May 27; 487(2):444–9. Available from: https://pubmed.ncbi.nlm.nih.gov/28427941/ PMID: 28427941
- 93. Bitan GM, Kirkitadze D, Lomakin A, Vollers SS, Benedek GB, Teplow DB. Amyloid β-protein (Aβ) assembly: Aβ40 and Aβ42 oligomerize through distinct pathways. Proc Natl Acad Sci U S A [Internet]. 2003 Jan 7; 100(1):330–5. Available from: www.pnas.orgcgidoi10.1073pnas.222681699 PMID: 12506200
- 94. You JC, Jones E, Cross DE, Lyon AC, Kang H, Newberg AB, et al. Association of β-amyloid burden with sleep dysfunction and cognitive impairment in elderly individuals with cognitive disorders. JAMA Netw open [Internet]. 2019 Oct 2; 2(10):e1913383. Available from: /pmc/articles/PMC6806437/. https://doi.org/10.1001/jamanetworkopen.2019.13383 PMID: 31617927
- 95. Solanas G, Peixoto FO, Perdiguero E, Jardí M, Ruiz-Bonilla V, Datta D, et al. Aged stem cells reprogram their daily rhythmic functions to adapt to stress. Cell [Internet]. 2017 Aug 10; 170(4):678–692. e20. Available from: http://www.ncbi.nlm.nih.gov/pubmed/28802040 PMID: 28802040
- 96. Yin Z, Raj D, Saiepour N, Van Dam D, Brouwer N, Holtman IR, et al. Immune hyperreactivity of Aβ plaque-associated microglia in Alzheimer's disease. Neurobiol Aging [Internet]. 2017; 55:115–22. Available from: http://www.sciencedirect.com/science/article/pii/S0197458017300970 PMID: 28434692
- Tansey KE, Cameron D, Hill MJ. Genetic risk for Alzheimer's disease is concentrated in specific macrophage and microglial transcriptional networks. Genome Med [Internet]. 2018 Feb 26; 10(1):14. Available from: https://www.ncbi.nlm.nih.gov/pubmed/29482603 PMID: 29482603
- Jastrebova N, Vanwildemeersch M, Rapraeger AC, Gimé Nez-Gallego G, Lindahl U, Spillmann D. Heparan sulfate-related oligosaccharides in ternary complex formation with fibroblast growth factors 1 and 2 and their receptors. J Biol Chem [Internet]. 2006; 281(37):26884–92. Available from: https://pubmed.ncbi.nlm.nih.gov/16807244/ PMID: 16807244
- 99. Kreuger J, Spillmann D, Li J, Lindahl U. Interactions between heparan sulfate and proteins: the concept of specificity. J Cell Biol [Internet]. 2006 Jul 31; 174(3):323–7. Available from: https://doi.org/10.1083/jcb.200604035 PMID: 16880267
- 100. Stopschinski BE, Holmes BB, Miller GM, Manon VA, Vaquer-Alicea J, Prueitt WL, et al. Specific gly-cosaminoglycan chain length and sulfation patterns are required for cell uptake of tau versus -synuclein and -amyloid aggregates. J Biol Chem [Internet]. 2018; 293(27):10826–40. Available from: http://dx.doi.org/10.1074/jbc.RA117.000378 PMID: 29752409
- 101. Narindrasorasak S, Lowery D, Gonzalez-DeWhitt P, Poorman RA, Greenberg B, Kisilevsky R. High affinity interactions between the Alzheimer's beta-amyloid precursor proteins and the basement membrane form of heparan sulfate proteoglycan. J Biol Chem [Internet]. 1991; 266(20):12878–83. Available from: http://www.sciencedirect.com/science/article/pii/S0021925818987764. PMID: 1906461
- 102. Schulz JG. Evidence that glypican is a receptor mediating β-amyloid neurotoxicity in PC12 cells. Eur J Neurosci [Internet]. 1998; 10(6):2085–93. Available from: https://pubmed.ncbi.nlm.nih.gov/9753095/PMID:9753095

- 103. Fuki I V., lozzo R V., Williams KJ. Perlecan heparan sulfate proteoglycan: A novel receptor that mediates a distinct pathway for ligand catabolism. J Biol Chem [Internet]. 2000; 275(33):25742–50. Available from: http://dx.doi.org/10.1074/jbc.M909173199 PMID: 10818109
- 104. Yanagishita M. Cellular catabolism of heparan sulfate proteoglycans. Trends Glycosci Glycotechnol [Internet]. 1998; 10(52):57–63. Available from: http://www.jstage.jst.go.jp/article/tigg1989/10/52/10_52_57/ article/-char/ja/.
- 105. Wyss-Coray T, Loike JD, Brionne TC, Lu E, Anankov R, Yan F, et al. Adult mouse astrocytes degrade amyloid-β in vitro and in situ. Nat Med [Internet]. 2003 Apr 1; 9(4):453–7. Available from: http://www.nature.com/naturemedicine PMID: 12612547
- 106. Kanekiyo T, Zhang J, Liu Q, Liu CC, Zhang L, Bu G. Heparan sulphate proteoglycan and the low-density lipoprotein receptor-related protein 1 constitute major pathways for neuronal amyloid-β uptake. J Neurosci [Internet]. 2011; 31(5):1644–51. Available from: https://www.jneurosci.org/content/31/5/1644 PMID: 21289173
- 107. Bishop JR, Schuksz M, Esko JD. Heparan sulphate proteoglycans fine-tune mammalian physiology [Internet]. Vol. 446, Nature. Nature Publishing Group; 2007. p. 1030–7. https://www.nature.com/ articles/nature05817.
- 108. Huang Y, Happonen KE, Burrola PG, O'Connor C, Hah N, Huang L, et al. Microglia use TAM receptors to detect and engulf amyloid β plaques. Nat Immunol [Internet]. 2021 Apr 15; 22(5):1–9. Available from: http://www.nature.com/articles/s41590-021-00913-5.
- 109. Baik SH, Kang S, Son SM, Mook-Jung I. Microglia contributes to plaque growth by cell death due to uptake of amyloid β in the brain of Alzheimer's disease mouse model. Glia [Internet]. 2016 Dec 1; 64(12):2274–90. Available from: https://onlinelibrary.wiley.com/doi/full/10.1002/glia.23074 PMID: 27658617
- 110. Weldon DT, Rogers SD, Ghilardi JR, Finke MP, Cleary JP, O'Hare E, et al. Fibrillar β-amyloid induces microglial phagocytosis, expression of inducible nitric oxide synthase, and loss of a select population of neurons in the rat CNS in vivo. J Neurosci [Internet]. 1998 Mar 15; 18(6):2161–73. Available from: https://www.jneurosci.org/lookup/doi/10.1523/JNEUROSCI.18-06-02161.1998 PMID: 9482801
- 111. Kandimalla KK, Scott OG, Fulzele S, Davidson MW, Poduslo JF. Mechanism of neuronal versus endothelial cell uptake of Alzheimer's Disease amyloid β protein. Cookson MR, editor. PLoS One [Internet]. 2009 Feb 27; 4(2):e4627. Available from: https://dx.plos.org/10.1371/journal.pone.0004627 PMID: 19247480
- 112. Omtri RS, Davidson MW, Arumugam B, Poduslo JF, Kandimalla KK. Difference in the cellular uptake and intracellular itineraries of amyloid beta proteins 40 and 42; ramifications for the Alzheimer's drug discovery. Bone [Internet]. 2012; 9(7):1887–97. Available from: https://www.ncbi.nlm.nih.gov/pmc/articles/PMC3858471/.
- 113. Wesén E, Jeffries GDM, Matson Dzebo M, Esbjörner EK. Endocytic uptake of monomeric amyloid-β peptides is clathrin- and dynamin-independent and results in selective accumulation of Aβ(1–42) compared to Aβ(1–40). Sci Rep [Internet]. 2017 Dec 17; 7(1):2021. Available from: http://www.nature.com/articles/s41598-017-02227-9 PMID: 28515429
- 114. Edwards IJ, Xu H, Obunike JC, Goldberg IJ, Wagner WD. Differentiated macrophages synthesize a heparan sulfate proteoglycan and an oversulfated chondroitin sulfate proteoglycan that bind lipoprotein lipase. Arterioscler Thromb Vasc Biol [Internet]. 1995 Mar; 15(3):400–9. Available from: https:// www.ahajournals.org/doi/10.1161/01.ATV.15.3.400 PMID: 7749850
- Miller JD, Cummings J, Maresh GA, Walker DG, Castillo GM, Ngo C, et al. Localization of perlecan (or a perlecan-related macromolecule) to isolated microglia in vitro and to microglia/macrophages following infusion of beta-amyloid protein into rodent hippocampus. Glia [Internet]. 1997 Oct 1; 21(2):228–43. Available from: https://doi.org/10.1002/(SICI)1098-1136(199710)21:2%3C228::AID-GLIA6%3E3. 0.CO PMID: 9336237
- 116. Kress GJ, Liao F, Dimitry J, Cedeno MR, FitzGerald GA, Holtzman DM, et al. Regulation of amyloid-β dynamics and pathology by the circadian clock. J Exp Med [Internet]. 2018 Apr 1; 215(4):1059–68. Available from: /pmc/articles/PMC5881473/. https://doi.org/10.1084/jem.20172347 PMID: 29382695
- 117. Ori A, Wilkinson MC, Fernig DG. A systems biology approach for the investigation of the heparin/ heparan sulfate interactome. J Biol Chem [Internet]. 2011; 286(22):19892–904. Available from: http:// www.sciencedirect.com/science/article/pii/S0021925820510648 PMID: 21454685
- 118. Swart M, Troeberg L. Effect of polarization and chronic inflammation on macrophage expression of heparan sulfate proteoglycans and biosynthesis enzymes. J Histochem Cytochem [Internet]. 2019 Jan 1; 67(1):9–27. Available from: https://doi.org/10.1369/0022155418798770 PMID: 30205019
- 119. Chen S, Fuller KK, Dunlap JC, Loros JJ. A Pro- and Anti-inflammatory axis modulates the macrophage circadian clock. Front Immunol [Internet]. 2020 May 14; 11:867. Available from: /pmc/articles/PMC7240016/. https://doi.org/10.3389/fimmu.2020.00867 PMID: 32477351

- 120. Lindahl U, Li J. Chapter 3 Interactions between heparan sulfate and proteins—Design and functional implications. In: International Review of Cell and Molecular Biology [Internet]. Academic Press; 2009. p. 105–59. https://linkinghub.elsevier.com/retrieve/pii/S1937644809760034 PMID: 19584012
- 121. Zhang X, Wang B, Li J-P. Implications of heparan sulfate and heparanase in neuroinflammation. Matrix Biol [Internet]. 2014 Apr; 35:174–81. Available from: https://linkinghub.elsevier.com/retrieve/pii/S0945053X13001777 PMID: 24398134
- 122. Zheng B, Albrecht U, Kaasik K, Sage M, Lu W, Vaishnav S, et al. Nonredundant roles of the mPer1 and mPer2 genes in the mammalian circadian clock. Cell [Internet]. 2001 Jun 1; 105(5):683–94. Available from: https://pubmed.ncbi.nlm.nih.gov/11389837/ PMID: 11389837
- 123. Balsalobre A, Damiola F, Schibler U. A serum shock induces circadian gene expression in mammalian tissue culture cells. Cell [Internet]. 1998 Jun 12; 93(6):929–37. Available from: http://www.cell.com/article/S009286740081199X/fulltext PMID: 9635423
- 124. Curtis AM, Bellet MM, Sassone-Corsi P, O'Neill LAJ. Circadian clock proteins and immunity. Immunity [Internet]. 2014; 40(2):178–86. Available from: http://www.sciencedirect.com/science/article/pii/S1074761314000405 PMID: 24560196